



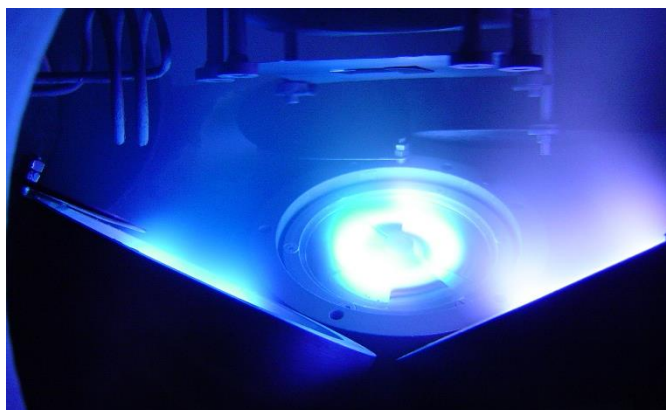
# Simulation par dynamique moléculaire Pulvérisation plasma/ion Réactions en phase gazeuse/plasma dépôts / croissance sous plasma

Pascal Brault  
GREMI UMR7344 CNRS – Université d'Orléans  
14, rue d'Issoudun BP6744  
45067 ORLEANS Cedex 2, France

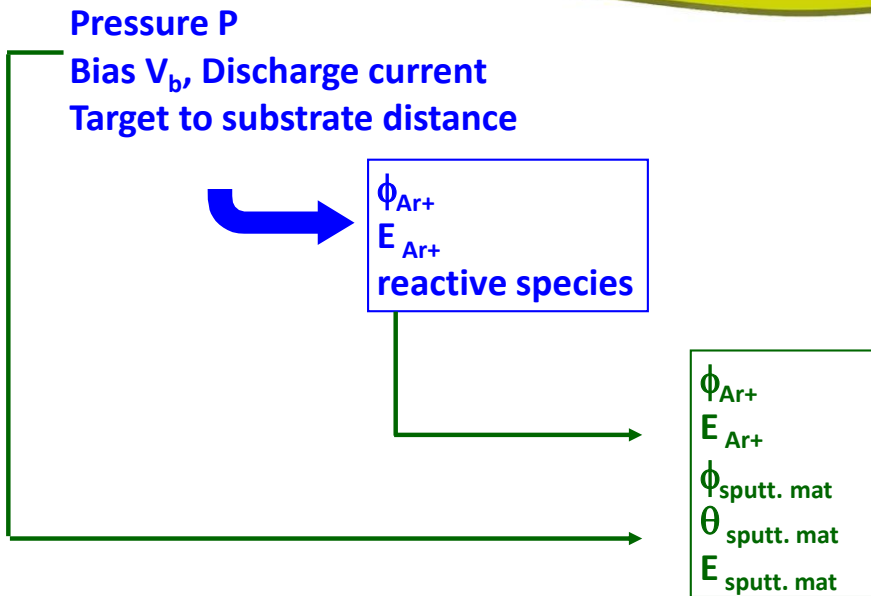
[pascal.brault@univ-orleans.fr](mailto:pascal.brault@univ-orleans.fr)



- ✓ (Reactive) Magnetron sputtering as an atom (molecule, cluster) source
- ✓ Molecular Dynamics principles
- ✓ Molecular Dynamics of sputtering
- ✓ Molecular Dynamics of gas phase reactions
- ✓ Molecular Dynamics of deposition
- ✓ Conclusions/Perspectives



# Deposition Parameters For Plasma Process Control



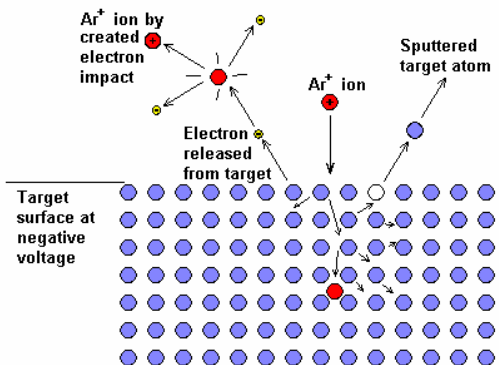
## Sputtering

Ion flux :  $1 \text{ A} = 6.25 \cdot 10^{18} \text{ s}^{-1}$   
 $4'' \text{ target} \Rightarrow \phi_{\text{ion}} \approx 10^{17} \text{ cm}^{-2} \text{ s}^{-1}$   
 sputtering rate  $\gamma(V_b) \approx 0.01 - 3$

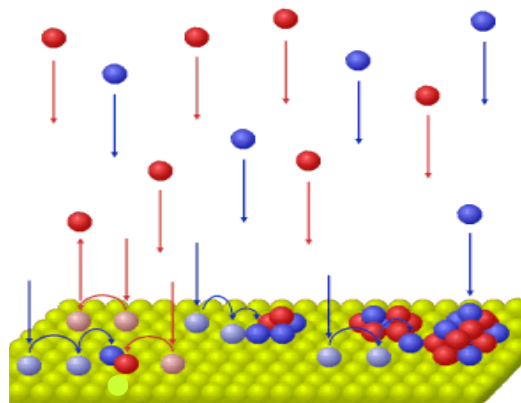
## Sputtered atom deposition

$\phi_{\text{atom}} \approx 10^{15} \text{ at cm}^{-2} \text{ s}^{-1}$   
 Sticking coefficient : 0.01 - 1  
 condensation

### Sputtering step

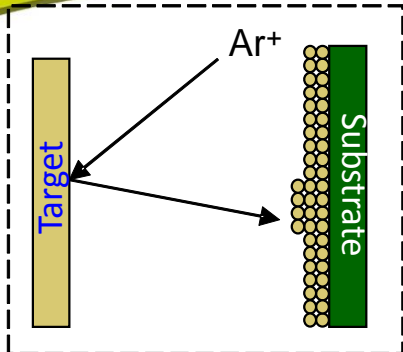


### Deposition step



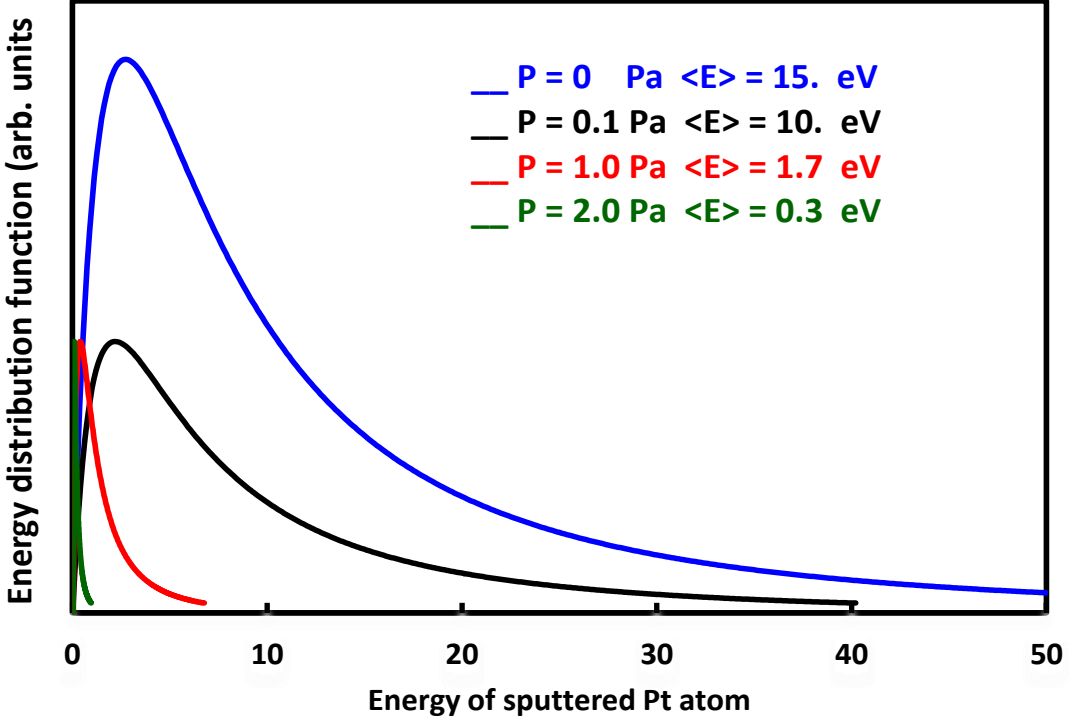
sputtering and deposition  
 ⇒ atomic scale processes  
 ⇒ MD is suitable

# Plasma sputtering: A controlled atom source



atom sources:

vapor at  $T_g$  (gas or evaporation : MB dist. of velocities),  
 Molecular beams ( $E_k \approx 0.01 - 10 \text{ eV} + T_g$ )  
 Sputtering (plasma, ion beam)  
 → Thompson distribution of sputtered atoms



## Sputtered Pt atom energy distribution

Target – substrate distance = 10 cm, Bias 300 V

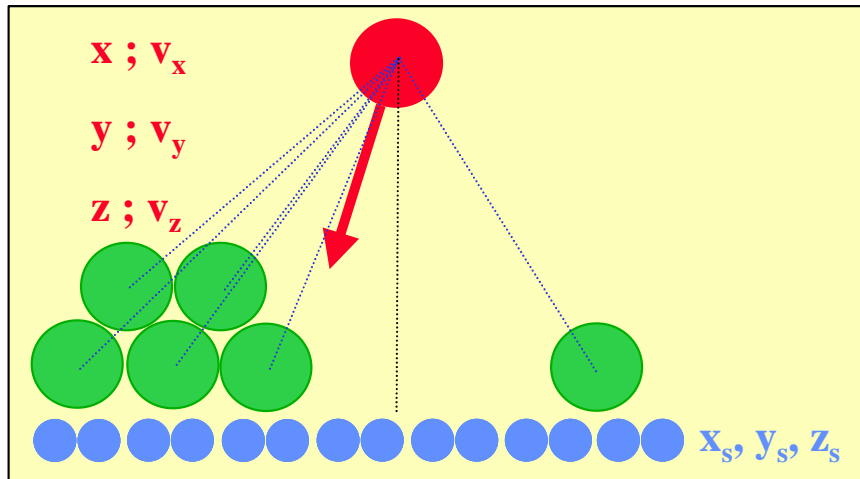
$$f(E) \propto \frac{1 - \left( \frac{E_{coh} + E}{\Delta E_{Ar^+}} \right)^{\frac{1}{2}}}{E^2 \left( 1 + \frac{E_{coh}}{E} \right)^3}$$

$$E_F = (E - k_B T_g) \exp[n \ln(E_f / E_i)] + k_B T_g$$

$$n = \frac{d_{T-S} P \sigma}{k_B T_g}$$

Pressure effect on energy distribution:  
 $P \nearrow f(E) \rightarrow \text{MB}, \forall f(E) \text{ and then } \langle E \rangle \searrow$

## Molecular Dynamics: Solving equations of motion :



$$m_j \frac{\partial^2}{\partial t^2} x_j = -\frac{\partial}{\partial x_j} V_s - \sum_{i \neq j} \frac{\partial}{\partial x_j} V_{ij}$$

$$m_j \frac{\partial^2}{\partial t^2} y_j = -\frac{\partial}{\partial y_j} V_s - \sum_{i \neq j} \frac{\partial}{\partial y_j} V_{ij}$$

$$m_j \frac{\partial^2}{\partial t^2} z_j = -\frac{\partial}{\partial z_j} V_s - \sum_{i \neq j} \frac{\partial}{\partial z_j} V_{ij}$$

Velocity Verlet algorithm: universally stable.

$$v(t + \frac{1}{2} \Delta t) = v(t) + \frac{1}{2} a(t) \Delta t$$

$$r(t + \Delta t) = r(t) + v(t + \frac{1}{2} \Delta t) \Delta t$$

*Force calculation a(t+Δt)*

$$v(t + \Delta t) = v(t + \frac{1}{2} \Delta t) + \frac{1}{2} a(t + \Delta t) \Delta t$$

All the trajectories and deduced (statistical) quantities are depending on the interaction potentials:

- DFT and ab-initio initial parametrization
- Semi-empirical model → ad-hoc functions parametrized on macroscopic properties:  
lattice parameter, cohesive energy, surface energy, angles, elastic constants, bonds, ...

*D. B. Graves & P. Brault, Molecular dynamics for low temperature plasma-surface interaction studies, J. Phys. D 42 (2009) 194011*  
*S. Erkoc, Empirical potential energy functions used in the simulations of materials properties, Annual Reviews of Computational Physics IX (2001) 1-103*

Additive pairwise interactions:

Lennard-Jones potential

$$U_{ij} = 4\epsilon \left[ \left( \frac{\sigma}{r_{ij}} \right)^{12} - \left( \frac{\sigma}{r_{ij}} \right)^6 \right]$$

Morse potential

$$U_{ij} = D [e^{-2\alpha(r_{ij}-r_0)} - 2e^{-\alpha(r_{ij}-r_0)}]$$

Buckingham potential

$$V_{ij}(r_{ij}) = A \exp\left(-\frac{r_{ij}}{r_B}\right) - \frac{C_6}{r_{ij}^6}$$

Molière potential

$$V_M(r_{ij}) = \frac{Z_1 Z_2 e^2}{4\pi \varepsilon_0 r_{ij}} \sum_{i=1}^3 c_i \exp\left(-d_i \frac{r_{ij}}{a_F}\right)$$

and ZBL potential  
(rare gas - surface  
and short range part)

$$V_{ZBL}(r_{ij}) = \frac{Z_1 Z_2 e^2}{4\pi \varepsilon_0 r_{ij}} \sum_{i=1}^4 c_i \exp\left(-d_i \frac{r_{ij}}{a_U}\right)$$

$$a_F = \frac{0.83 \left(\frac{9\pi^2}{128}\right)^{1/3} a_B}{\left(Z_1^{1/2} + Z_2^{1/2}\right)^{2/3}} \quad \text{and} \quad a_U = \frac{0.8853 a_B}{(Z_1^{0.23} + Z_2^{0.23})}$$

with  $a_B = 0.529\ 177\text{ \AA}$

# Molecular Dynamics Simulations

## Potentials

Species	Morse potential			L-J potential		Buckingham potential		
	$D_0$ (eV)	$\alpha$ ( $\text{\AA}^{-1}$ )	$r_0$ ( $\text{\AA}$ )	$\varepsilon$ ( $\text{\AA}$ )	$\sigma$ (eV)	A (eV)	$r_B$ ( $\text{\AA}$ )	$C_6$ (eV $\text{\AA}^6$ )
Ag	0.3294	1.3939	3.096		0.392	2.62		
Al			—	0.01	3.4			
Ar			—	0.449	2.637			
Au	0.4826	1.6166	3.004					
Ba	0.1416	0.656 98	5.373					
C			—	3.4	$2.41 \times 10^{-3}$			
Ca	0.1623	0.805 35	4.569	0.215				
Cr	0.4414	1.5721	2.754	0.502				
Cs	0.044 85	0.415 69	7.557					
Cu	0.3446	1.3921	2.864	0.409				
Fe	0.4216	1.3765	2.849	0.527				
Ga	—	—				5902.871	0.3187	250.0
He			—	$8.81 \times 10^{-4}$	2.56			
In	—	—				6141.774	0.3567	258.0
Ir	0.8435	1.6260	2.864					
K	0.054 24	0.497 67	6.369	0.114				
Kr			—	0.014	4.285			
Li			—	0.205	3.65			
Mo	0.7714	1.434	3.012	0.838				
N	10.56	2.557	1.097			5134.176	3.140	283.8
Na	0.063 34	0.589 93	5.336	0.1379				
Nb	0.9437	1.5501	3.079					
Ne			—	$3.13 \times 10^{-3}$	2.74			
Ni	0.4279	1.3917	2.793	0.520				
O	5.12	2.68	1.208					
Pb	0.2455	1.2624	3.667	0.236				
Pd	0.4761	1.6189	2.89	0.427				
Pt	0.7102	1.6047	2.897	0.685				
Rb	0.046 44	0.429 81	7.207					
Rh	0.6674	1.5423	2.875					
Sr	0.1513	0.73776	4.988					
W	0.9710	1.385	3.053	1.068				
Xe			—	0.02	2.562			
			—	3.98				
AlN						698.647	0.3224	0.0
GaN						782.107	0.3166	0.0
InN						870.207	0.3263	0.0

<i>i</i>	$c_i$	$d_i$
<i>Moliere</i>		
1	0.35	0.3
2	0.55	1.2
3	0.1	6.0
<i>ZBL</i>		
1	0.028 17	0.201 62
2	0.280 22	0.402 90
3	0.509 86	0.942 29
4	0.181 75	3.199 80

## 3-body Potentiels but quasi pairwise screened Vashishta potential

$$\Phi = \phi_2 + \phi_3 = \sum_{i < j} U_{ij} + \sum_{i < j < k} W_{ijk},$$

$$U_{ij} = \frac{H_{ij}}{r_{ij}^{\eta_{ij}}} + \frac{Z_i Z_j}{r_{ij}} e^{-r_{ij}/r_{1s}} - \frac{P_{ij}}{r_{ij}^4} e^{-r_{ij}/r_{4s}},$$

$$H_{ij} = A_{ij}(\sigma_i + \sigma_j)^{\eta_{ij}},$$

$$P_{ij} = \frac{1}{2}(\alpha_i Z_j^2 + \alpha_j Z_i^2).$$

f radius is  $r_c$ .

$$W_{ijk} = B_{ijk} f(r_{ij}, r_{ik})(\cos \theta_{ijk} - \cos \bar{\theta}_{ijk})^2,$$

$$f(r_{ij}, r_{ik}) = \exp \left( \frac{l}{r_{ij} - r_{c3}} + \frac{l}{r_{ik} - r_{c3}} \right); \quad r_{ij}, r_{ik} < r_{c3},$$

$$\cos \theta_{ijk} = \frac{\mathbf{r}_{ik} \cdot \mathbf{r}_{ij}}{r_{ij} r_{ik}}; \quad r_{ij}, r_{ik} < r_{c3}.$$

	$A_{ij}$ (erg)	$r_{1s}$ (Å)	$r_{4s}$ (Å)	$r_c$ (Å)	$\ell$ (Å)	$r_{c3}$ (Å)
SiO <sub>2</sub>	$1.242 \times 10^{-12}$	4.43	2.5	5.5	1.0	2.6
Si <sub>3</sub> N <sub>4</sub>	$2.00 \times 10^{-12}$	2.5	2.5	5.5	1.0	2.6
$\sigma_i$ (Å)		$Z_i$ (e)	$\alpha_i$ (Å <sup>3</sup> )			
Si	0.47	1.20	0.00			
O	1.20	-0.60	2.40			
Si	0.47	1.472	0.00			
N	1.30	-1.104	3.00			
	$\eta_{ij}$			$B_{jik}$ (erg)		$\theta_{jik}$ (°)
Si-Si	11			Si-O-Si	$3.20 \times 10^{-11}$	141.00
Si-O	9			O-Si-O	$0.80 \times 10^{-11}$	109.47
O-O	7					
Si-Si	11			Si-N-Si	$2.0 \times 10^{-11}$	120.00
Si-N	9			N-Si-N	$1.0 \times 10^{-11}$	109.47
N-N	7					

P. Vashishta, & al, in *Amorphous Insulators and Semiconductors*, eds. M. F. Thorpe and M. I. Mithova, NATOASI Series 3, Vol. 23 (Kluwer, 1997), p. 151

### N-body reactive potential REBO family

$$V_{ij}(r_{ij}) = f_c(r_{ij}) \{ V_R(r_{ij}) - b_{ij} V_A(r_{ij}) \}$$

$$V_A(r) = \frac{D_0}{S-1} \exp \left[ -\beta \sqrt{2S} (r - R_0) \right],$$

$$V_R(r) = \frac{D_0 S}{S-1} \exp \left[ -\beta \sqrt{\frac{2}{S}} (r - R_0) \right].$$

	Tersoff (Si)	Tersoff (C)	Brenner (C)	BN	NN	BB
$D_0$ (eV)	2.666	5.1644	6.325	6.36	9.91	3.08
$R_0$ (Å)	2.295	1.447	1.315	1.33	1.11	1.59
$S$	1.4316	1.5769	1.29	1.0769	1.0769	1.0769
$\beta$ (Å <sup>-1</sup> )	1.4656	1.9640	1.5	2.043 057	1.927 871	1.524 4506
$\gamma$	$1.1 \times 10^{-6}$	$1.5724 \times 10^{-7}$	$1.1304 \times 10^{-2}$	$1.1134 \times 10^{-5}$	0.019 251	$1.6 \times 10^{-6}$
$n$	0.787 34	0.727 51	1 ( $1/2n = 0.804 69$ )	0.364 153 367	0.618 4432	3.992 9061
$c$	$1.0039 \times 10^5$	$3.8049 \times 10^4$	19	1092.9287	17.7959	0.526 29
$d$	16.217	4.384	2.5	12.38	5.9484	0.001 587
$h$	-0.598 25	-0.570 58	-1	0.5413	0	0.5
$\lambda$	0	0	0	1.9925	0	0
$R$ (Å)	2.85	1.95	1.85	2.0	2.0	2.0
$D$ (Å)	0.15	0.15	0.15	0.1	0.1	0.1

$$f_c(r) = \begin{cases} \frac{1}{2} - \frac{1}{2} \sin \left[ \frac{\pi}{2} \frac{r-R}{D} \right] & (r < R-D) \\ 0 & R-D < r < R+D, \\ & r \geqslant \end{cases}$$

ou bien

$$f_c(r) = \frac{1}{1 + \exp[(r - R)/D]}.$$

$$\chi_{ij} = \sum_{k(\neq i,j)}^N f_c(r_{ik}) g(\theta_{ijk}) \exp[\lambda^3 (r_{ij} - r_{ik})^3)],$$

$$g(\theta_{ijk}) = 1 + \frac{c^2}{d^2} - \frac{c^2}{d^2 + (h - \cos \theta_{ijk})^2}$$

Tight binding – 2<sup>nd</sup> moment approximation

(transition métals → catalysts)

True N-body potential : CPU time consuming

	Ni	Cu	Rh	Pd	Ag	Ir	Pt	Au	Al	Pb
A	0.0376	0.0855	0.0629	0.1746	0.1028	0.1156	0.2975	0.2061	0.1221	0.0980
ξ	1.070	1.224	1.660	1.718	1.178	2.289	2.695	1.790	1.316	0.914
p	16.999	10.08	18.45	10.867	10.928	16.980	10.612	10.229	8.612	9.576
q	1.189	2.56	1.867	3.742	3.139	2.961	4.004	4.036	2.516	3.648

Parametrized up to 5th neighbour

F. Cleri et V. Rosato, Phys. Rev B48 (1993) 22

### Embedded Atom Method (EAM)

- ⇒ energy of a solid is a unique functional of the electron density.
- ⇒ uses the concept of electron (charge) density to describe metallic bonding:
- ⇒ each atom contributes through a spherical, exponentially-decaying field of electron charge, centered at its nucleus, to the overall charge density of the system.
- ⇒ Binding of atoms is modelled as embedding these atoms in this “pool” of charge, where the energy gained by embedding an atom at location  $r$  is some function of the local density.
- ⇒ The total energy thus writes:

$$E_{pot} = \sum_{i=1}^N E_i = \frac{1}{2} \sum_{i=1}^N \sum_{j,j,i \neq j}^N \phi_{ij}(r_{ij}) + \sum_{i=1}^N F_i(\rho_i) \quad \rho = \sum_{j,j \neq i}^N f_j(r_{ij})$$

With pairwise function:

$$\phi(r) = \frac{A \exp\left[-\alpha\left(\frac{r}{r_e} - 1\right)\right]}{1 + \left(\frac{r}{r_e} - \kappa\right)^{20}} - \frac{B \exp\left[-\beta\left(\frac{r}{r_e} - 1\right)\right]}{1 + \left(\frac{r}{r_e} - \lambda\right)^{20}}$$

$$f(r) = \frac{f_e \exp\left[-\beta\left(\frac{r}{r_e} - 1\right)\right]}{1 + \left(\frac{r}{r_e} - \lambda\right)^{20}}$$

And the embedding function:

$$F(\rho) = \sum_{i=0}^3 F_{ni} \left( \frac{\rho}{0.85\rho_e} - 1 \right)^i, \quad \rho < 0.85\rho_e$$

$$F(\rho) = \sum_{i=0}^3 F_i \left( \frac{\rho}{\rho_e} - 1 \right)^i, \quad 0.85\rho_e \leq \rho < 1.15\rho_e$$

$$F(\rho) = F_n \left[ 1 - \eta \ln \left( \frac{\rho}{\rho_s} \right) \right] \left( \frac{\rho}{\rho_s} \right)^\eta, \quad \rho \geq 1.15\rho_e$$

**coupling rule**

$$\phi^{ab}(r) = \frac{1}{2} \left[ \frac{f^b(r)}{f^a(r)} \phi^{aa}(r) + \frac{f^a(r)}{f^b(r)} \phi^{bb}(r) \right]$$

reactive force field : ReaxFF

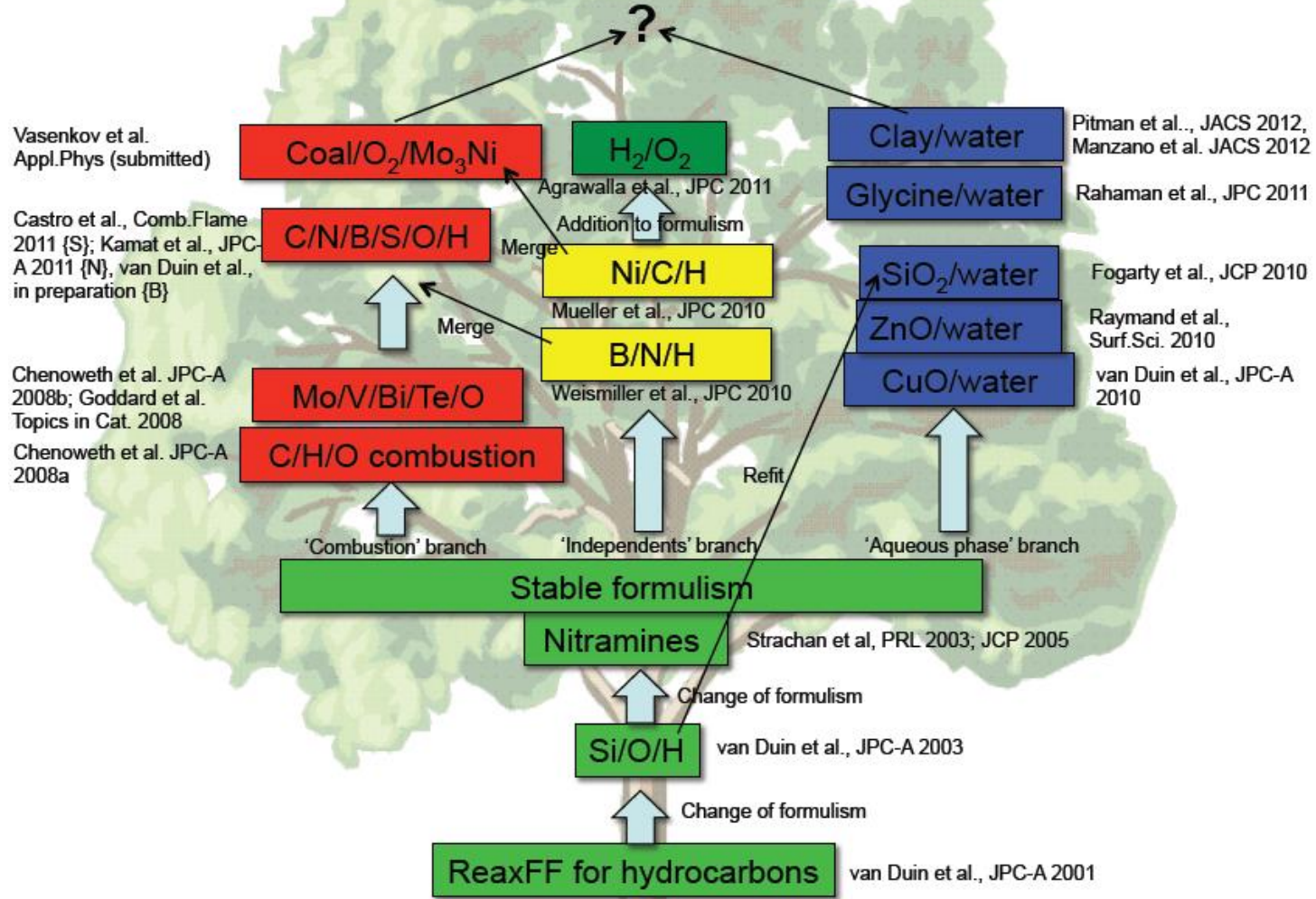
(based on distance angle relationship initially proposed by Tersoff/Brenner)

- To get a smooth transition from nonbonded to single, double and triple bonded systems ReaxFF employs a bond length/bond order relationship [1-3]. Bond orders are updated every iteration.
- All connectivity-dependent interactions (i.e. valence and torsion angles, H-bond) are made bond-order dependent, ensuring that their energy contributions disappear upon bond dissociation.
- Nonbonded interactions (van der Waals, Coulomb) are calculated between every atom pair, irrespective of connectivity. Excessive close-range nonbonded interactions are avoided by shielding.
- ReaxFF uses EEM, a geometry-dependent charge calculation scheme that accounts for polarization effects [4].

1. Brenner, D. W., (1990) Physical Review B **42**, 9458-9471
2. Tersoff, J., (1988) Physical Review Letters **61**, 2879-2882.
3. Abell, G. C., (1985) Physical Review B **31**.
4. Mortier, W. J., Ghosh, S. K., and Shankar, S. (1986) JACS **108**, 4315-4320.

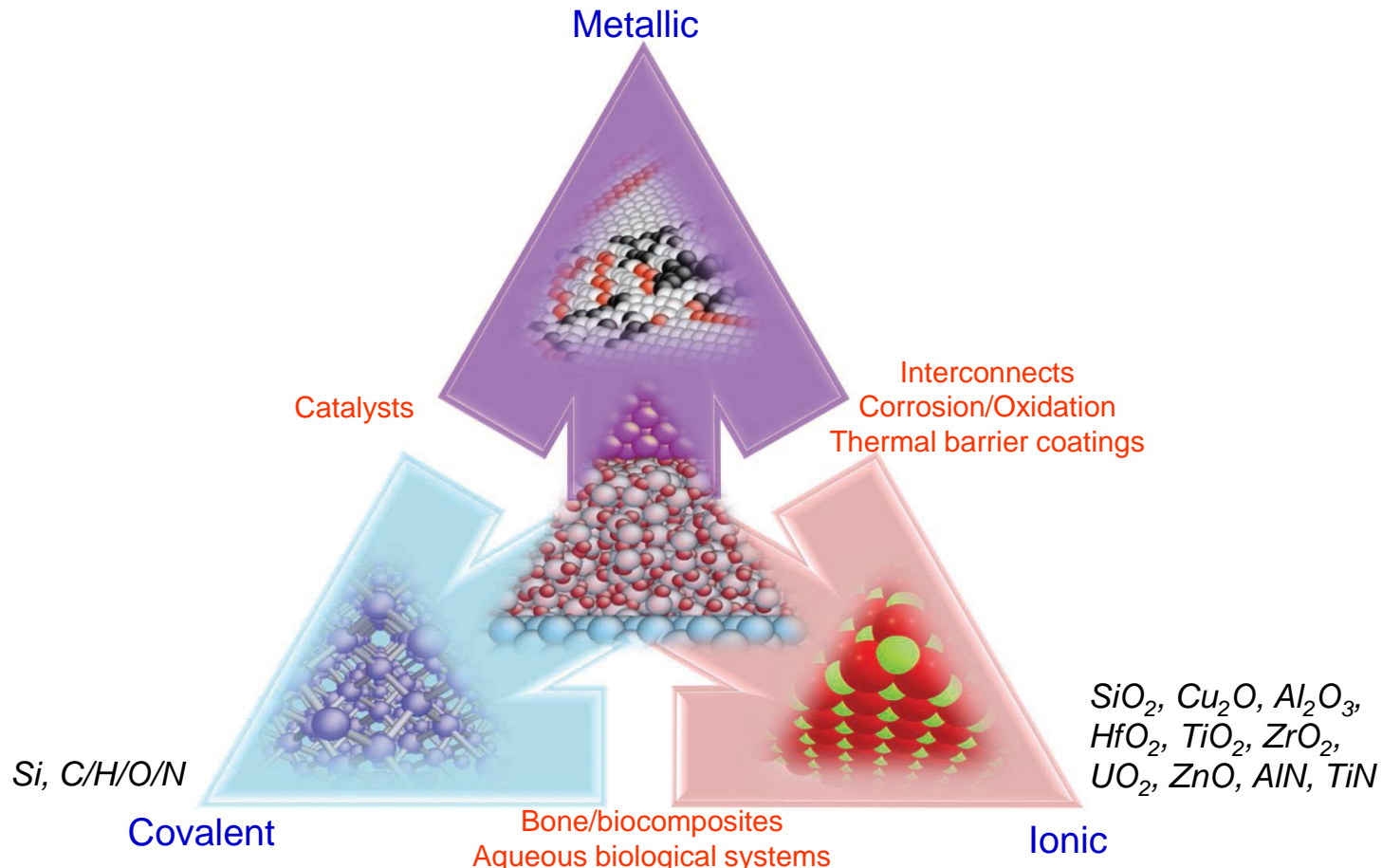
<http://www.engr.psu.edu/adri>

## ReaxFF development tree: towards complex materials



Charge Optimized Many Body (COMB) Potential :  
adapted to ionic interaction with variable charges

## Visual presentation of COMB potentials



# Functional form of COMB potential

- Functional form of COMB potential:

- $$E_T = \sum_i \left[ E_i^S(q_i) + \frac{1}{2} \sum_{j \neq i} V_{ij}(r_{ij}, q_i, q_j) + C(r_{ij}, q_i, q_j) \right]$$

- Self energy: fit to atomic ionization energies and electron affinities

$$E_i^S(q_i) = \chi_i q_i + (J_i + J_i^{field}) q_i^2 + K_i q_i^3 + L_i q_i^4$$

- Interatomic potential: Charge dependent Tersoff + Coulomb

$$V_{ij}(r_{ij}, q_i, q_j) = f_c(r_{ij}) \cdot A_{ij}(q_i, q_j) \cdot e^{-\lambda_{ij} \cdot r_{ij}} - f_c(r_{ij}) \cdot b_{ij} \cdot B_{ij}(q_i, q_j) \cdot e^{-\alpha_{ij} \cdot r_{ij}} + q_i \cdot J_{ij}(r_{ij}) \cdot q_j$$

- Spherical charge distribution: 1s-type Slater orbital

- $$J_{ij}(r_{ij}) = n_{ij} \int d^3 r_i \int d^3 r_j \rho_i(r_i, q_i) \rho_j(r_j, q_j) / r_{ij}$$

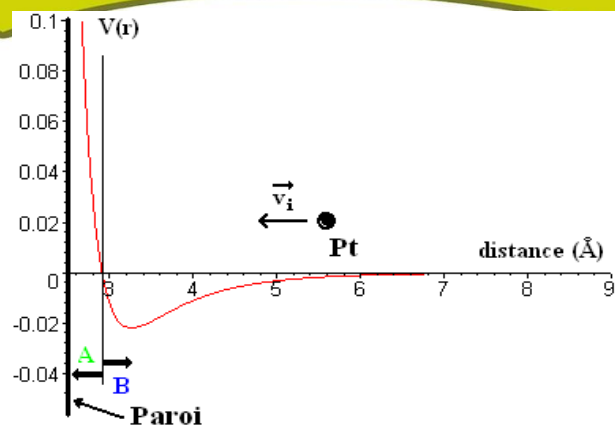
- $$\rho_i(r_i, q_i) = q_i \frac{\xi_i^3}{\pi} \exp(-2\xi_i |r - r_i|)$$

<sup>1</sup> J. Yu, et. al., *Phys. Rev. B* **75** 085311 (2007)

<sup>2</sup> T.-R. Shan, et al., *Phys. Rev. B* **81**, 125328 (2010)

### Thermalisation model

As  $\vec{F} \cdot \vec{v} < 0$ , or some relevant criterion, the velocity should be rescaled during some times  $\Rightarrow$  thermostat



Collision is modelled by a coupling (electron-phonon, for metals)  
which introduces friction term in Newton equations of motion  $\Rightarrow$  Langevin

$$\frac{\partial^2 \vec{r}_i(t)}{\partial t^2} = -\frac{1}{m_i} \frac{\partial}{\partial \vec{r}} V(\vec{r}_1(t), \vec{r}_2(t), \dots, \vec{r}_N(t)) - \mu \vec{v}_i(t)$$

$$\mu = m_s \alpha \frac{T_i - T_e}{T_i} \quad \text{et} \quad \alpha = \frac{\Theta_D T_e L n e^2 k_B Z}{2 m_e \kappa \epsilon_F}$$

$\alpha^{-1}$  is the thermalisation time

For example, Pt:  $\alpha^{-1} = 1.17$  ps

Au:  $\alpha^{-1} = 20$  ps

Q. Hou et al, Phys. Rev. B 62 (2000) 2825

other ways:

- velocity rescaling (Berendsen thermostat) :

$$v \rightarrow \chi v \text{ with: } \chi = \left( 1 + \frac{dt}{\tau} \left( \frac{T_s}{T_k} - 1 \right) \right)^{\frac{1}{2}}$$

$\tau$  is the thermal relaxation time.

$T_s$  is the targeted temperature (surface),

$T_k$  is the kinetic temperature:  $E_k = kT_k \approx \frac{1}{2} mv^2$

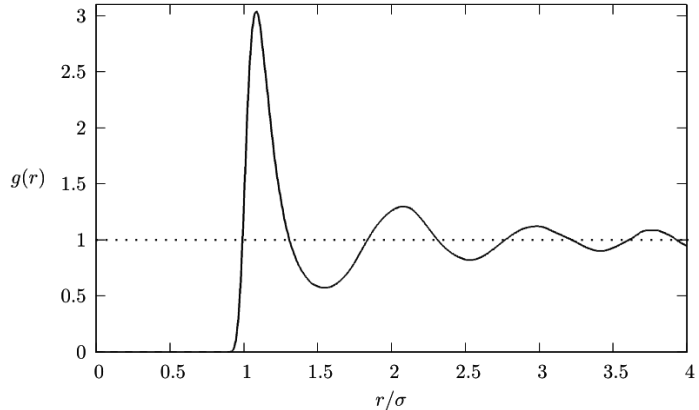
- Langevin thermostat :

$$m\ddot{\mathbf{r}}(t) = -m\Omega^2 \mathbf{r}(t) - \nabla_{\mathbf{r}} W(\mathbf{r}, \mathbf{R}) - m\beta \dot{\mathbf{r}}(t) + \mathbf{f}(t),$$

$$M\ddot{\mathbf{R}}(t) = -\nabla_{\mathbf{R}} W(\mathbf{r}, \mathbf{R}),$$

- Radial distribution function : Atom number between distances  $r$  and  $r+dr$ :

$$\int_0^{\infty} \rho g(r) 4\pi r^2 dr = N - 1 \approx N$$



- Concentration profile of:
  - sputtering gas in the target, reactive species poisoning of the target
  - sputtered (reacted) materials on/in a substrate
- Size distribution (in flight or on a substrate)
- Diffusion coefficient :  $D = \frac{1}{\delta} \lim_{t \rightarrow \infty} \frac{d\langle |r_i(t) - r_i(t_0)|^2 \rangle}{dt}$
- ... many other things ...

- Simulated X-ray patterns of:
  - (reactively) sputtered target
  - sputtered (reacted) film or clusters on/in a substrate
- Debye formula for calculating XRD patterns:

$$I_k(b) = \sum_n \sum_{n \neq m} f_n(b) f_m(b) \frac{\sin(2\pi b r_{nm})}{2\pi b r_{nm}}$$

$b=2\sin(\theta)/\lambda$  and  $\lambda$  is the wavelength of the incident radiation,  $2\theta$  is the scattering angle, and  $r_{nm}$  is the distance between atoms n and m. The functions  $f_n(b)$  and  $f_m(b)$  are the scattering factors for atoms n and m, respectively

Pioneering work : H. M. Urbassek et al:

## Molecular-dynamics simulation of sputtering

Herbert M. Urbassek

Fachbereich Physik, Universität Kaiserslautern, Erwin-Schrödinger-Straße, D-67663 Kaiserslautern, Germany

Nuclear Instruments and Methods in Physics Research B 122 (1997) 427–441

Boundary between low and high kinetic energy  $E_k = 100$  eV  $\Rightarrow$  if  $> 100$ eV par repulsive potential (binary collision) as Molière, ZBL, Kr-C

Describe collision cascade  $E_k > 1$  keV

Studies mostly concerned by Ion Beam Sputtering ...

... a bit different than plasma sputtering

- lower energy range 10 to 500 eV
- buffer gas  $\Rightarrow$  collisions :
  - Energy distribution function is modified
  - molecules, clusters formation

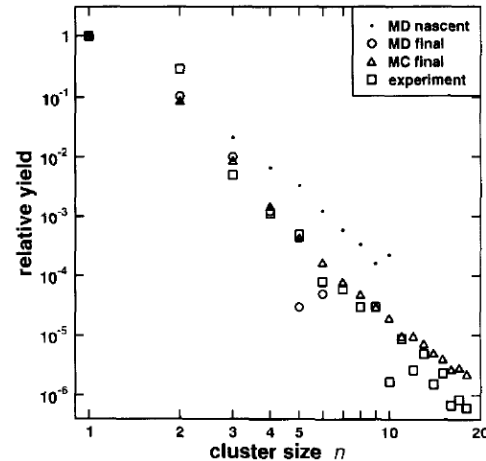


Fig. 5. Relative abundance distribution  $Y(n)$  of  $\text{Ag}_n$  clusters sputtered from a Ag (111) surface due to 5 keV Ar bombardment. Nascent and final distributions calculated by molecular dynamics immediately after, and 500 ps after ion emission. Monte Carlo results, extrapolated from molecular-dynamics data as described in the text. Experimental data from Ref. [157]. Plotted after Ref. [59] with permission of the author.

### Available computer codes

**Table 1.1.** Computer codes used in the fields of ion-implantation and ion-surface interactions

6

T. Ono et al.

Slowing Down Process				Thermal Process	
Binary Collision Approximation				Molecular Dynamics	
Simple MC	Dynamical MC			MDACOCT <sup>24</sup>	MD-TOPS <sup>26</sup>
ACAT <sup>1</sup>	ACOCT <sup>5</sup>	TRIDYN <sup>10</sup>	EVOLVE <sup>12</sup>	PARASOL <sup>25</sup>	SPUT2SI <sup>29</sup>
TRIM <sup>2</sup>	MARLOWE <sup>6</sup>	T-DYN <sup>11</sup>	dynamical-	MODYSEM <sup>27</sup>	SPUT3 <sup>28</sup>
TRIM.SP <sup>3</sup>	Crystal-TRIM <sup>7</sup>		SASAMAL <sup>13</sup>	MOLDYCASK <sup>30</sup>	QDYN <sup>32</sup>
SASAMAL <sup>4</sup>	COSIPO <sup>8</sup>	DynamO : <a href="http://dynamomd.org/">http://dynamomd.org/</a>		MOLDY <sup>31</sup>	REED <sup>33</sup>
	IMSIL <sup>9</sup>		DYACAT <sup>14</sup>	DYACOCT <sup>15</sup>	
			ACAT-DIFFUSE <sup>19</sup>	ACAT-DIFFUSE-GAS <sup>20</sup>	EDDY <sup>23</sup> TMAP4 <sup>18</sup>
			TRIDYN+PIDAT <sup>21</sup>	TRIDYN+DIFFUSED-C+YCEHM <sup>22</sup>	

- (1) Y. Yamamura and Y. Mizuno, Research report of Institute of Plasma Physics, Nagoya University IPPJ-AM-40 (1985).
- (2) J.P. Biersack and L.G. Haggmark, Nucl. Instr. Meth. 174 (1980) 257.
- (3) J.P. Biersack and W. Eckstein, Appl. Phys. A34 (1984) 73.
- (4) Y. Miyagawa and S. Miyagawa, J. Appl. Phys. 54 (1983) 7124.
- (5) Y. Yamamura and W. Takeuchi, Nucl. Instrum. Methods B29 (1987) 461.
- (6) M.T. Robinson and I.M. Torrens, Phys. Rev. B9 (1974) 5008.
- (7) M. Posselt, Radiat. Eff. Def. Solid. 130/131 (1994) 87.
- (8) M. Hautala, Phys. Rev. B30 (1984) 5010.
- (9) G. Hobler, H. Potzl, L. Gong and H. Ryssel, in: Simulation of Semiconductor Devices and Process, eds. W. Fichtner and D. Aemmer, Vol. 4 (Hartung-Gorre, Konstanz, 1991) p.389.
- (10) W. Möller and W. Eckstein, Nucl. Instr. Meth. B 2 (1984) 814.
- (11) J.P. Biersack, S. Berg and C. Nender, Nucl. Instr. Meth. B59–60 (1991) 21.
- (12) M.L. Roush, T.S. Andreadis and O.F. Goktepe, Radiat. Eff. 55 (1981) 119.
- (13) Y. Miyagawa, M. Ikeyama, K. Saitoh, G. Massouras, S. Miyagawa, J. Appl. Phys. 70 (1991) 7289.
- (14) Y. Yamamura, Nucl. Instrum. Methods B33 (1988) 493.
- (15) Y. Yamamura, I. Yamada and T. Takagi, Nucl. Instr. Meth. B37–38 (1989) 902.
- (16) K.L. Wilson and M.I. Baskes, J. Nucl. Mater. 76/77 (1978) 291.
- (17) W. Möller, Max-Plank-Institute für Plasmaphysik, Report IPP 9/44 (1983).
- (18) G.R. Longhurst, D.F. Holland, J.L. Jones, B.J. Merrill, TMAP4 User's Manual, EGG-FS-10315, Idaho National Engineering and Environmental Laboratory, 1992.
- (19) Y. Yamamura, Nucl. Instr. Meth. B 28 (1987) 17.
- (20) M. Ishida, Y. Yamaguchi and Y. Yamamura, Thin Solid Films 334 (1998) 225.
- (21) W. Eckstein, V.I. Shulga, J. Roth, Nucl. Instr. Meth. B 153 (1999) 415.
- (22) K. Schmid and J. Roth, J. Nucl. Mater. 313–316 (2003) 302.
- (23) K. Ohya and R. Kawakami, Jpn. J. Appl. Phys. 40 (2001) 5424.
- (24) K. Yorizane, T. Muramoto and Y. Yamamura, Nucl. Instr. Meth. B153 (1999) 292.
- (25) G. Betz, R. Kirchner, W. Husinsky, F. Rudenauer and H.M. Urbassek, Radiation Effects and Defects in Solids 130/131 (1994) 251.
- (26) Javier Domínguez-Vázquez, E. Pablo Andribet, A. Mari Carmen Pérez-Martín, José J. Jiménez-Rodríguez, Radiation Effects and Defects in Solids 142 (1997) 115.
- (27) V. Konoplev and A. Gras-marti, Philosophical magazine A71 (1995) 1265.
- (28) M.H. Shapiro and T.A. Tombrello, Nucl. Instr. Meth. B84 (1994) 453.
- (29) M.H. Shapiro, T.A. Tombrello and D.E. Harrison, Jr., Nucl. Instr. Meth. B30 (1988) 152.
- (30) T. Diaz de la Rubia and M.W. Guinan, J. Nucl. Mater. 174 (1990) 151.
- (31) B.L. Holian, The MOLDY program is filed in mass storage at the Los Alamos National Laboratory (1975).
- (32) D.E. Harrison, Jr. and M.M. Jakas, Radiat. Eff. 99 (1986) 153.
- (33) Jeong-Won Kang, E.S. Kang, M.S. Son, and H.J. Hwang, Journal of Vacuum Science & Technology B18 (2000) 458–461.

To what we have to pay special care in addition to the interaction potentials

Ion flux :

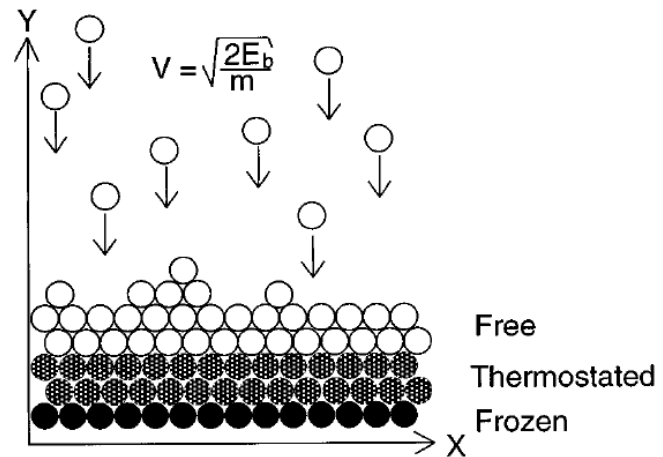
Exp.  $1 \text{ } 10^{17} \text{ cm}^{-2} \text{ s}^{-1}$  (\*) = 10 ions /  $10 \times 10 \text{ nm}^2 / \text{s}$  (\*) 1A on 4" target  
 MD 1 ion/ $10 \times 10 \text{ nm}^2 / 2 \text{ ps}$

Integration timestep dt

Evolves as  $dt = \frac{C}{\sqrt{\max_{1 \leq i \leq N} \left( \frac{2[E_{kin} + \max(0, V_i)]}{m_i} \right)}}$  ( $E < 1 \text{ eV} : dt \approx 1 \text{ fs}$ , except quick motion bonded H 0.1 fs)

Thermal relaxation

- Choose a relevant ion release time: i.e. greater than thermalisation time
- Choose a relevant thermostat (region i.e. what should thermostated) with this relevant time
- For sputtering one can guess that only a part of the substrate should be thermostated

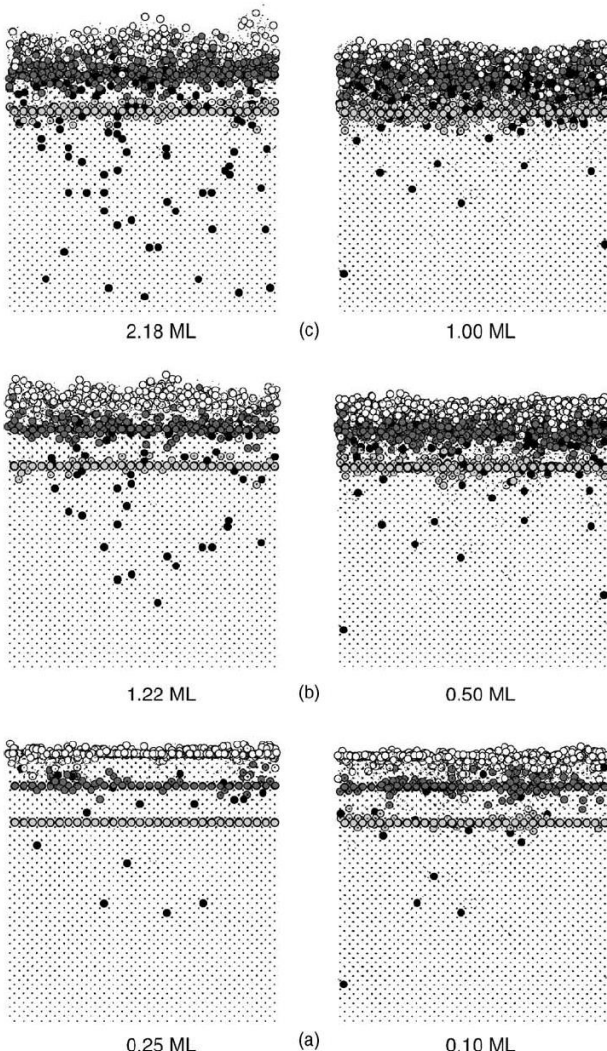


NB a neutral-atom potential is appropriate because the incident ion is neutralized well before impact by a fast Auger process or resonant charge transfer

# Molecular Dynamics Simulations Sputtering: effect of the potential

B.J. Thijssse et al./Applied Surface Science 231–232 (2004) 29–38

Molecular dynamics simulation of silicon sputtering: sensitivity to the choice of potential  
MEAM SW



Side-view snapshots of Si(001) targets irradiated by 500 eVAr atoms at 45° incidence, with doses (bottom to top):  
(a)  $0.48 \cdot 10^{14} \text{ Ar}/\text{cm}^2$ , (b)  $2:14 \cdot 10^{14} \text{ Ar}/\text{cm}^2$ , and (c)  $4:26 \cdot 10^{14} \text{ Ar}/\text{cm}^2$ .

The white, dark gray, and light gray circles represent the atoms initially in planes 1, 8, and 17, respectively (counted from the top),

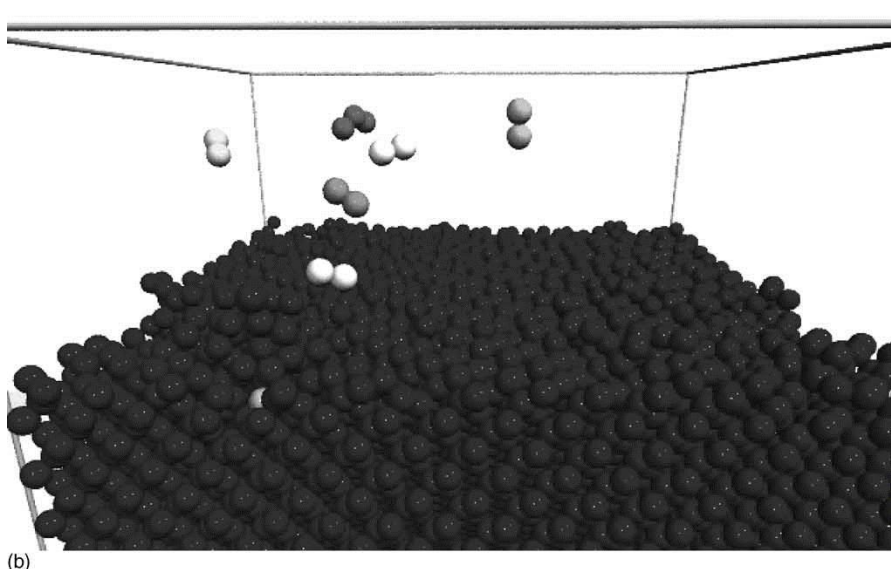
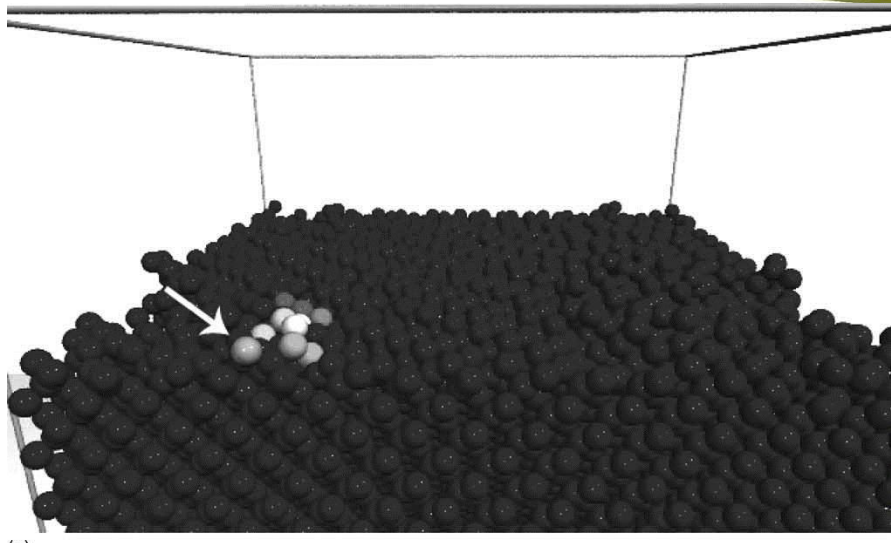
and the black circles are implanted Ar atoms.

All other atoms are represented by small dots.  
The left column shows the MEAM simulation results, the right column the SW results. Under each snapshot the number of sputtered monolayers is indicated.

SW Stillinger-Weber : Tersoff-like potential  
MEAM Modified EAM for including bond angles

# Molecular Dynamics Simulations

## Sputtering: effect of the potential



Sputter burst event occurring in the MEAM simulation:

- (a) situation just before Ar impact (arrow), highlighting the 13 Si atoms that will eventually be sputtered;
- (b) five Si dimers and one Si trimer ejected from the surface. The Ar atom is still visible in the surface region.

MEAM fitted to DFT results, but spurious thermal effects are occurring.

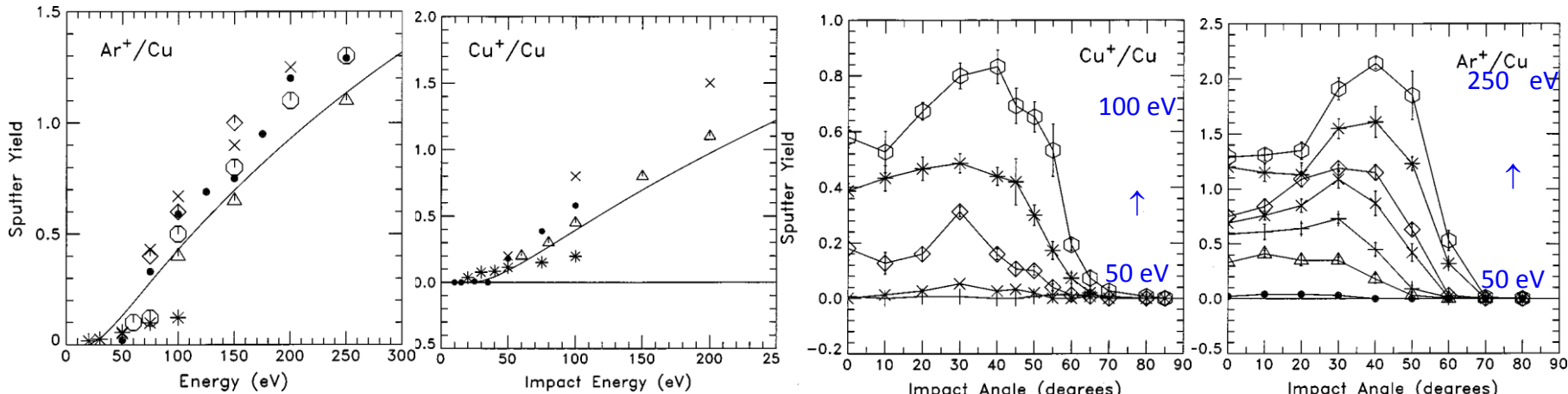
**Lesson:** even when using potentials that are well fitted to first-principles data, one should be extremely cautious and never stop validating (experimentally) results.

# Molecular Dynamics Simulations

## Sputtering: sputtered atom data

Molecular dynamics simulation of Cu and Ar ion sputtering of Cu (111) surfaces

J. D. Kress, D. E. Hanson, A. F. Voter, C. L. Liu, X.-Y. Liu, and D. G. Coronell, JVST A 17, 2819 (1999)



Experiments ( $\square$ ,  $\Delta$ ,  $\diamond$ ),  
empirical  
formula (—), binary collision (\*),  
previous MD simulation (x);  
present MD (•)

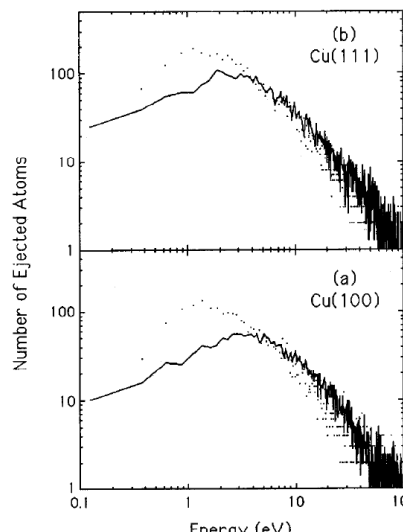
Comparison with experiment  
( $\Delta$ ), the formula of Yamamura *et*  
*al.* (—), the present MD  
simulation (•), the MD simulation  
of Shapiro and Tombrello (x), and  
binary collision simulation (\*)

### Potentials

Cu – Cu : EAM

Ar – Cu : ZBL

Ar – Ar : Molière.



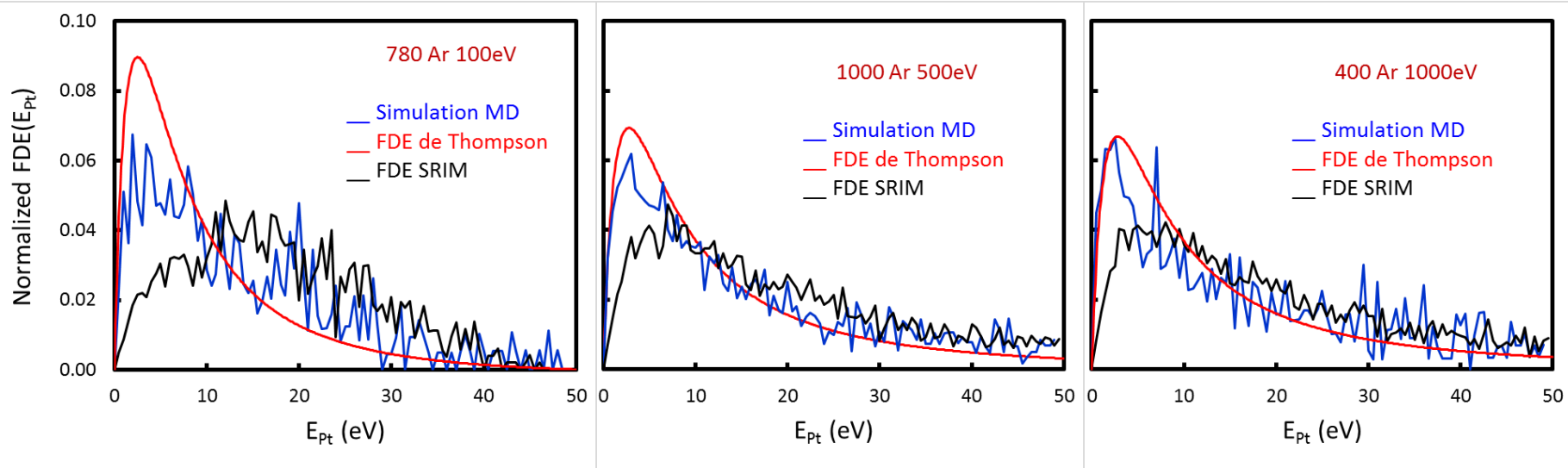
Energy distributions  
... pair potential  
— EAM potential

# Molecular Dynamics Simulations

## Sputtering: sputtered atom data

### Energy distribution functions (FDE) of sputtered materials

#### The case of Pt vs sputtering Ar kinetic energy

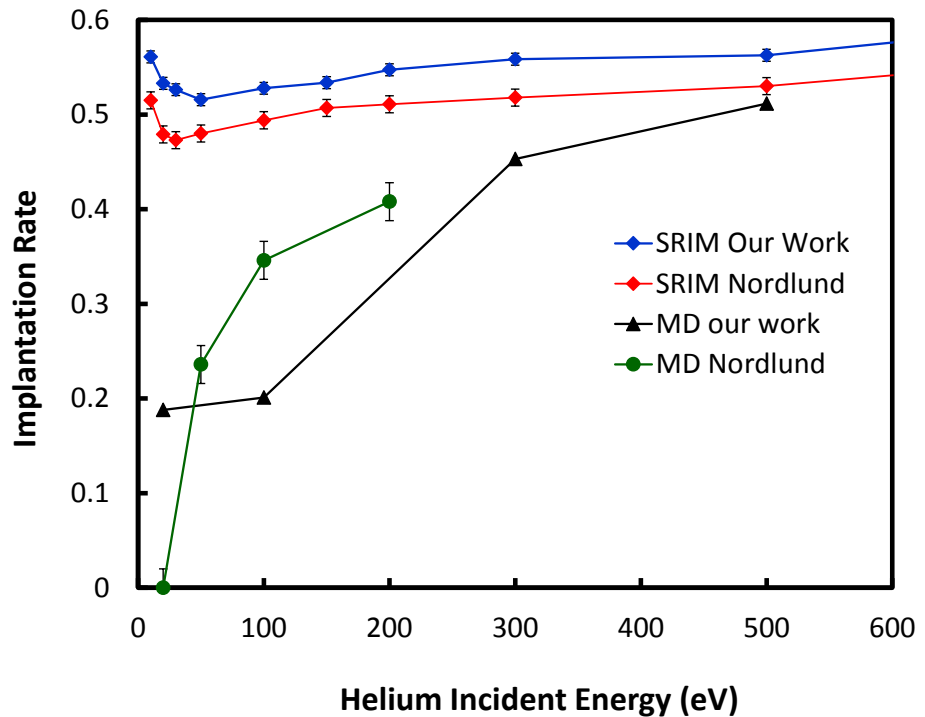


Low kinetic energy side of Thompson theory and high energy side of SRIM are recovering the MD energy distribution of sputtered Pt energy distribution function

(P. Brault, J.M. Bauchire, S. Chuon, 2015, unpublished)

# Molecular Dynamics Simulations beyond magnetron sputtering (I)

## Helium interaction with tungsten



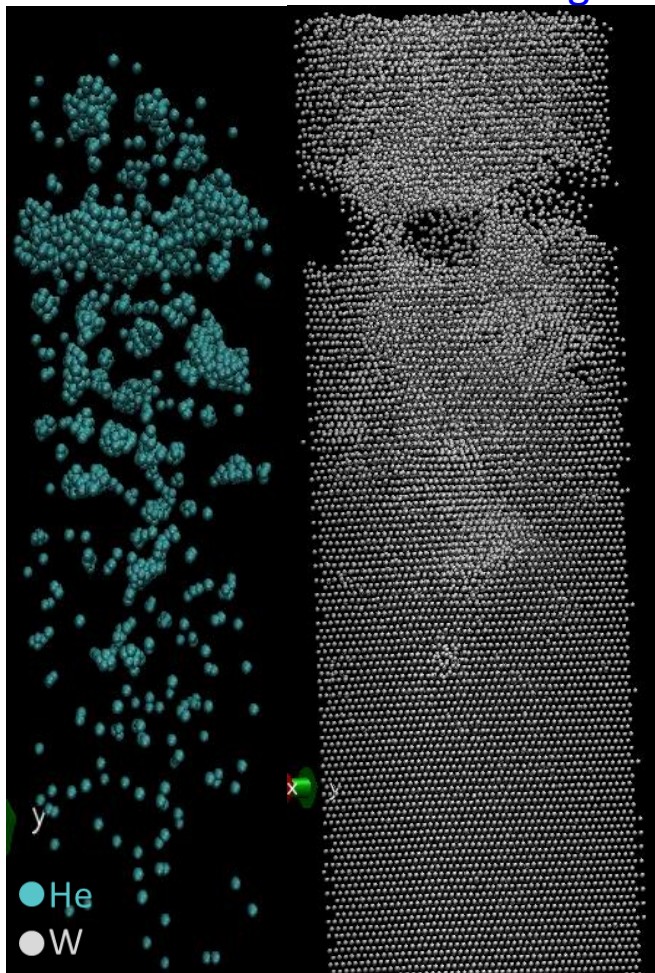
Discrepancy between MD and SRIM at low energies.

Discrepancy between MDs : HeW potentials

Our Work: Ph D thesis work of L. Pentecoste at GREMI

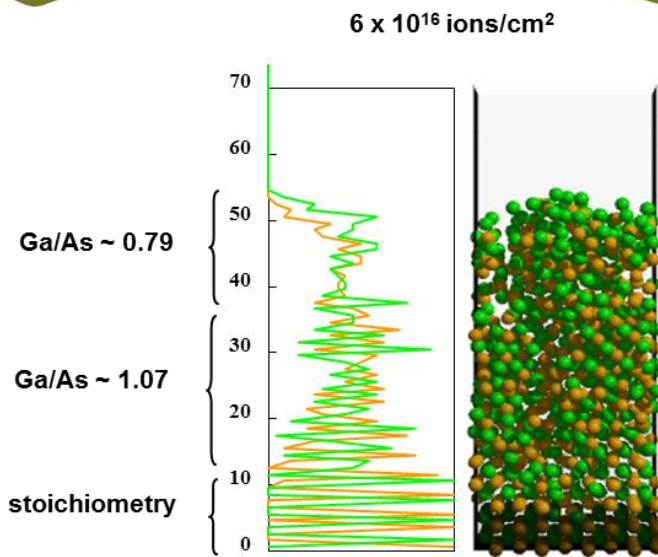
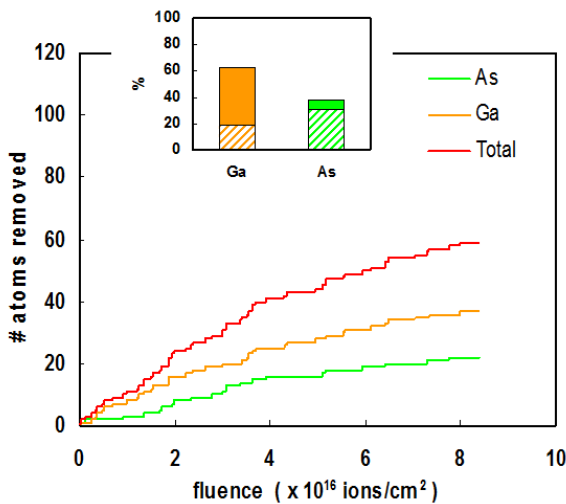
Nordlund: K.O.E. Henriksson, K. Nordlund, J. Keinonen , Molecular dynamics simulations of helium cluster formation in tungsten, Nuclear Instruments and Methods in Physics Research B 244 (2006) 377–391

## He bubble formation and W flaking off



# Molecular Dynamics Simulations beyond magnetron sputtering (II)

## Sputter etch: compound sputtering $\rightarrow \text{Ar}^+$ on GaAs



- Ga preferential sputtering and As cross-linking initially occur on top surface
- More than 97% of sputtered species are single atoms, in good agreement with experimental mass spectrometry studies\*
- Thermal desorption is necessary to get steady state

- Concentration profiles show a top surface enrichment of As, a subsurface depletion of As, then a return to stoichiometry deeper in the solid
- Good agreement with ARXPS and AES analyses\* of GaAs surfaces exposed to higher bombardment energies [0.5;5keV] but with Ga/As ratios closer to unity

Emilie Despiau-Pujo, Pascal Chabert, and David B. Graves, Molecular dynamics simulations of GaAs sputtering under low-energy argon ion bombardment, JVST A 26, 274 (2008)

# Molecular Dynamics Simulations reactive magnetron sputtering

None about this topics except reactive ion etching !!

Why ?

1/ complicated :

reactive species: neutral, radical, dissociation, ionisation

Target poisoning

molecule formation with sputtered materials

2/ problem with time and length scales

especially for reactivity during transport to substrate

-

3/ Availability of metal-oxide, nitride, carbide potentials

COMB ( $\text{TiO}_x$ ,  $\text{SiO}_x$ ,  $\text{AlO}_x$ ,  $\text{HfO}_x$ ,  $\text{ZnO}$ , ...)

and REBO (B, C, H, N, Si, O)

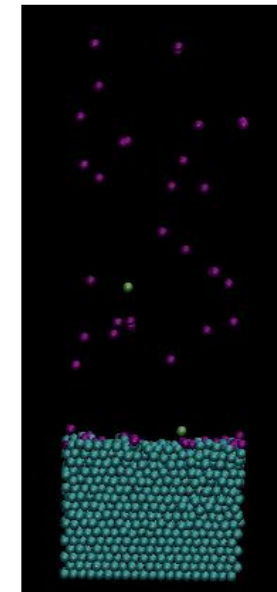
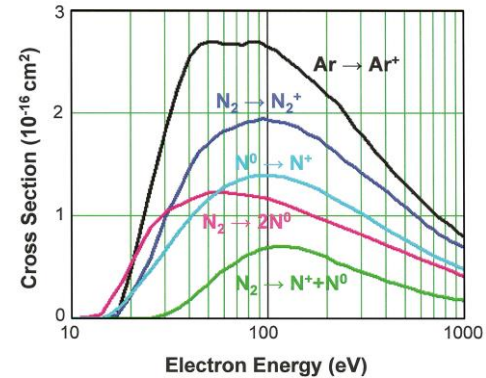
and ReaxFF (C, H, N, Si, O)

4/ how to ?

Ion flux:  $1 \cdot 10^{17} \text{ cm}^{-2} \text{s}^{-1}$   $\Rightarrow \frac{n_n}{n_i}$  above the surface  $\approx 1$  to  $100$

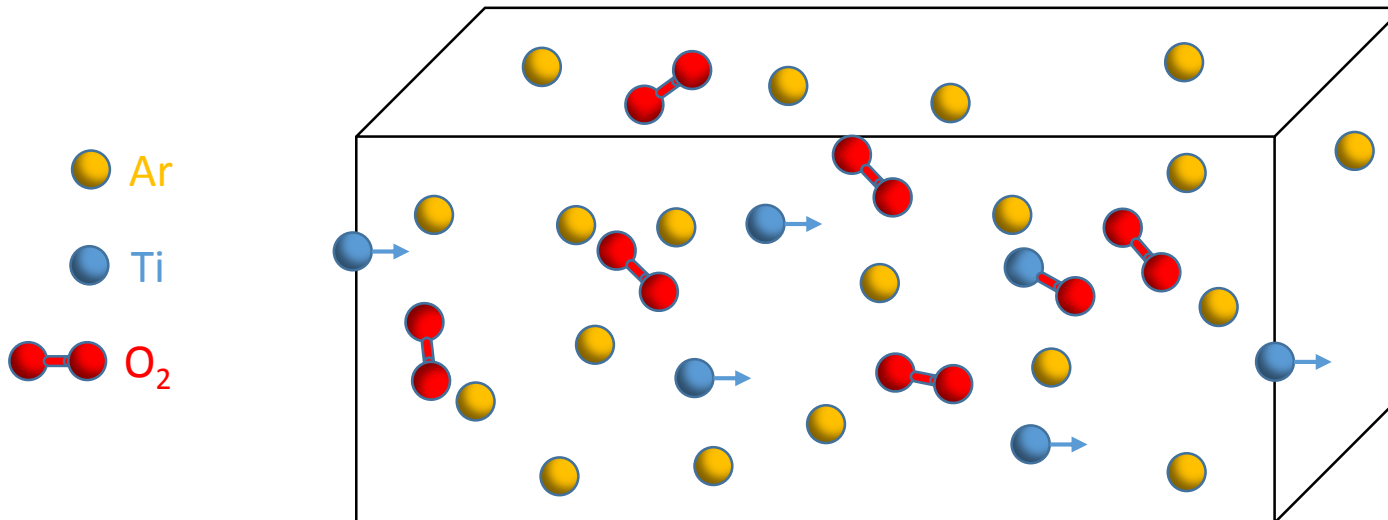
reactive neutral flux: few  $10^{17} \text{ cm}^{-2} \text{s}^{-1}$   $n_i$

Problem : how to describe molecule formation ?



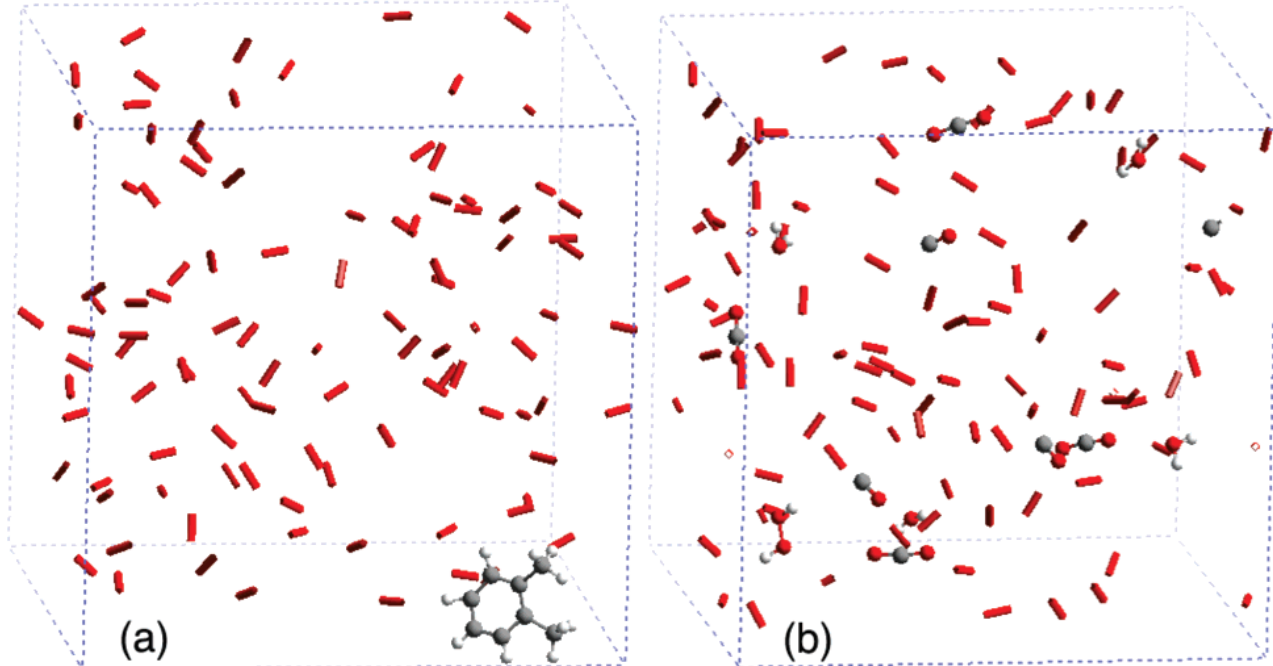
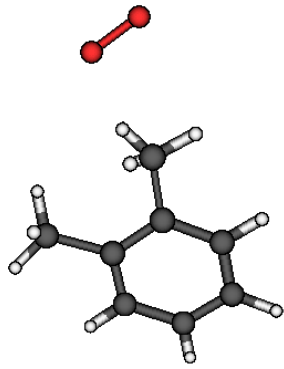
## Tricks:

- use P.d of the experiment and increase P and decrease d accordingly collision number being  $\propto P.d$
- Take into account that unreactive (Ar ?) buffer gas is able to dissipate energy towards reactor wall.  
Unreactive buffer gas density can be thus underestimated
- 3D boundary conditions for accounting traveling of buffer gas by fast sputtered atoms



# Molecular Dynamics Simulations Gas/plasma phase reactions

Example of gas phase reaction: oxidation of o-xylene



(a) Snapshot of the equilibrated o-xylene/O<sub>2</sub> system.

(b) Final configuration after an 1800 ps NVT-MD simulation was performed at 2500 K.

K. Chenoweth, A. C. T. van Duin, and W. A. Goddard III, *ReaxFF Reactive Force Field for Molecular Dynamics Simulations of Hydrocarbon Oxidation*, J. Phys. Chem. A 2008, 112, 1040

### Example of gas phase reaction: soot formation in plasma

Point de départ cohérent avec le modèle HACA (\*)  
mélange  $C_6H_5$  (radical phenyl) +  $C_2H_2$  (acétylène)

boîte de simulation :

$5 \times 5 \times 5 \text{ nm}^3$

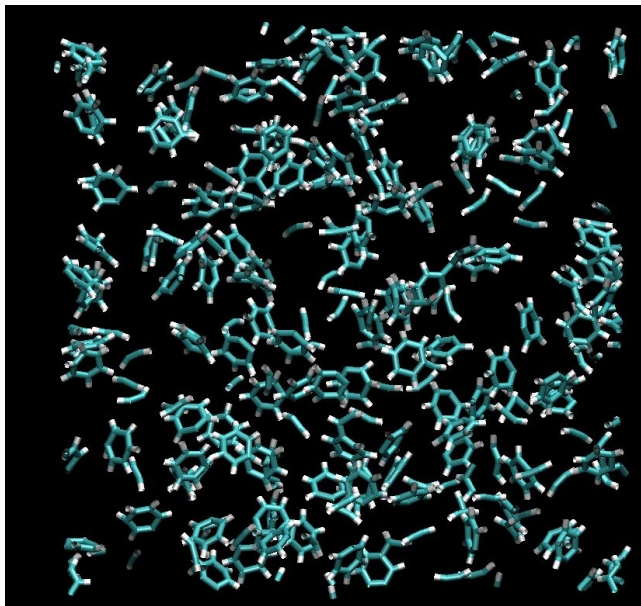
125 molécules de  $C_6H_5$

125 molécules de  $C_2H_2$

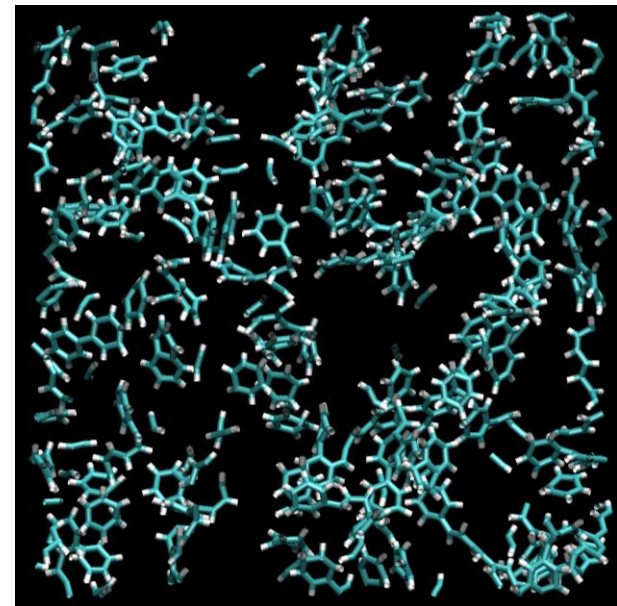
$dt = 0.1 \text{ fs}$ , Equilibrage NVT

Calcul NVE

On retrouve les espèces précurseur prévues dans le modèle Hassouni-Mohasseb (\*)



Etat initial



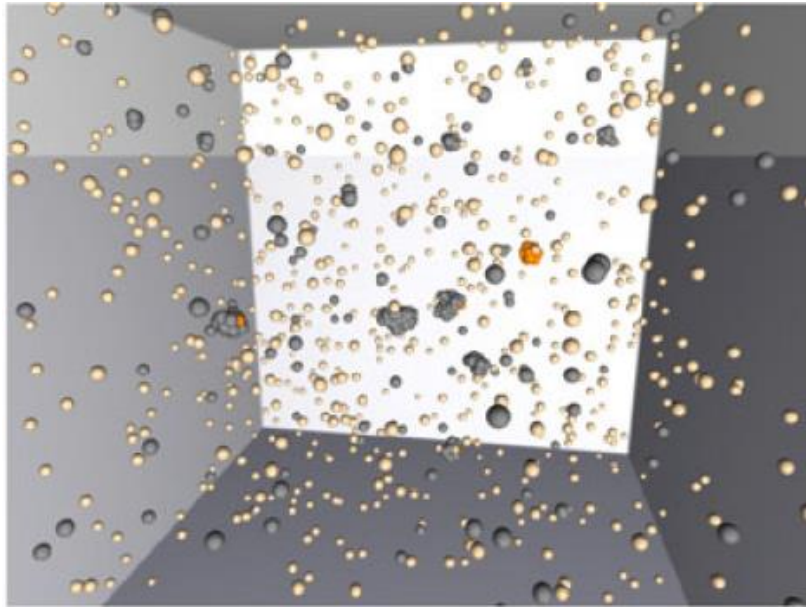
Etat à 500 ps

Tableau II. 1 : Structures de quelques hydrocarbures aromatiques polycycliques							
A1		A2					
Benzène		Naphtalène					
A3		A4					
Phénantrène		Pyrène					
A1C <sub>2</sub> H <sub>2</sub>		P2					
Phényl-acétylène		Bi-phényl					

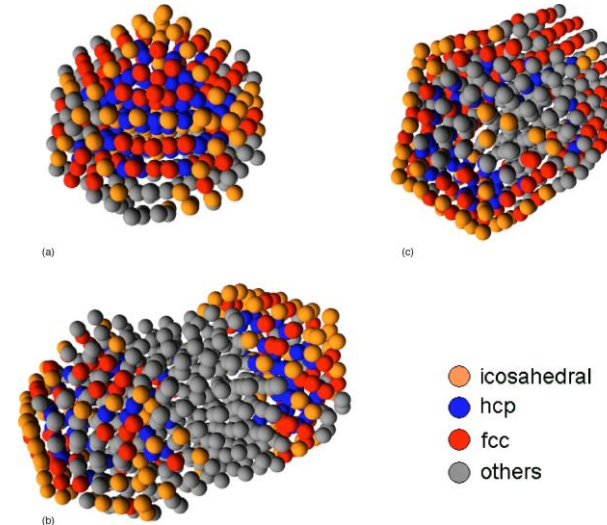
(\*) K. Hassouni, F. Mohasseb, F. Bénédic, G. Lombardi, and A. Gicquel, *Formation of soot particles in Ar/H<sub>2</sub>/CH<sub>4</sub> microwave discharges during nanocrystalline diamond deposition: A modeling approach*, Pure Appl. Chem. 78 (2006) 1127  
P. Brault (2014) unpublished

# Molecular Dynamics Simulations Condensation during the flight

If gas pressure large enough (as for gas condensation) clustering of sputtered atoms occurs during the flight to the surface



Snapshots of a simulation (800 K inert gas temperature, Ar:Fe 2:1,  $\rho(\text{Fe}) = 0.07 \text{ mol dm}^{-3}$ ) after 2.3 ns simulation time. Beige: argon; grey: iron in unordered structures, orange: iron in an icosahedral environment.



(a) The biggest cluster before the collision. (b) The new cluster 0.165 ns after the collision or at 16.4 ns of the overall simulation time. (c) The cluster at 11.3 ns after the collision or 27.5 ns of the overall simulation time.

N Lümmen, T Kraska, Investigation of the formation of iron nanoparticles from the gas phase by molecular dynamics simulation, *Nanotechnology* 15 (2004) 525–533; Molecular dynamics investigations of the coalescence of iron clusters embedded in an inert-gas heat bath, *Phys. Rev B* 71 (2005) 205403

# Molecular Dynamics Simulations

## Sputtering deposition

Focus on : high entropy alloys, metal oxides and CNT growth in plasma context  
 recall: Energy distribution of incoming species at the substrate position .

$$f(E) \propto \frac{1 - \left( \frac{E_{coh} + E}{\Lambda E_{Ar^+}} \right)^{\frac{1}{2}}}{E^2 \left( 1 + \frac{E_{coh}}{E} \right)^3}$$

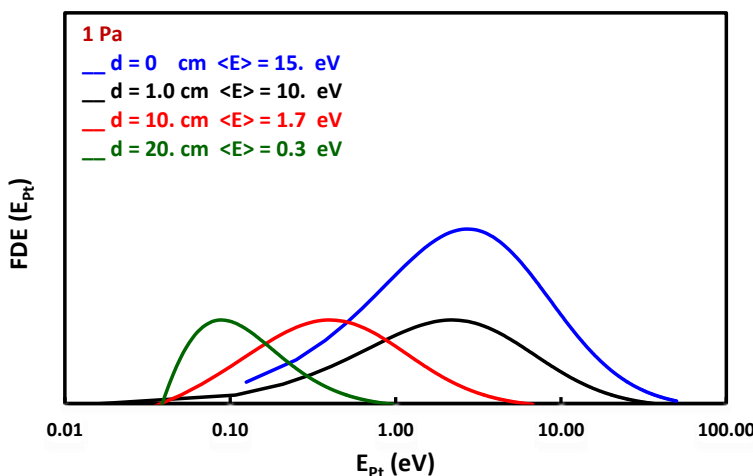
$$E_F = (E - k_B T_g) \exp[n \ln(E_f / E_i)] + k_B T_g$$

$$n = \frac{d_{T-S} P \sigma}{k_B T_g}$$

MD flux: 1 at/100nm<sup>2</sup>/2ps i.e. 0.5 at nm<sup>-2</sup> ps<sup>-1</sup>  
 Exp flux: 10<sup>15</sup> at cm<sup>-2</sup>s<sup>-1</sup> i.e. 10 at nm<sup>-2</sup>s<sup>-1</sup> !

So time between releasing each depositing atoms should be greater than thermalisation time : a few ps

Released total number: 10000 at.



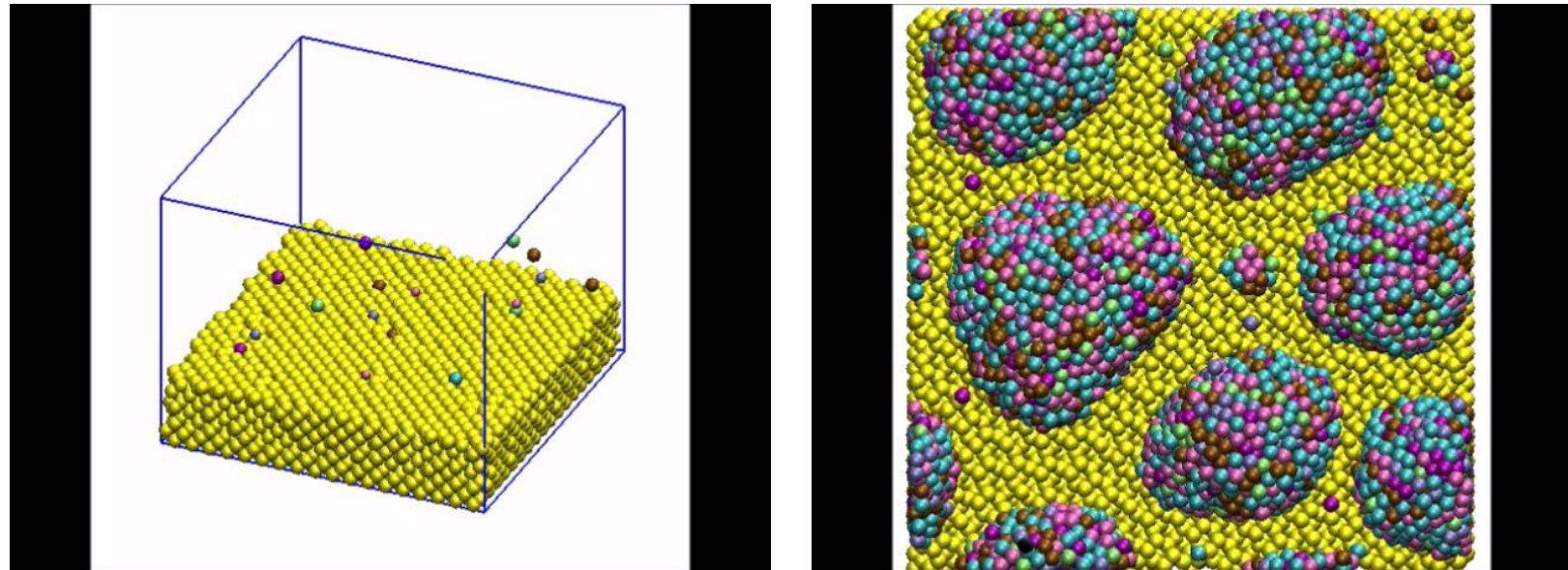
quasi equimolar AlCoCrCuFeNi deposition:

1309/1205/1293/1357/1348/1354 atoms  $\rightarrow$  Al<sub>17</sub>Co<sub>15</sub>Cr<sub>17</sub>Cu<sub>17</sub>Fe<sub>17</sub>Ni<sub>17</sub>

$\langle E \rangle = 1$  eV for each element

Sticking = 0.80 env.

Substrate Si(100)  $\approx$  100x100 Å<sup>2</sup>



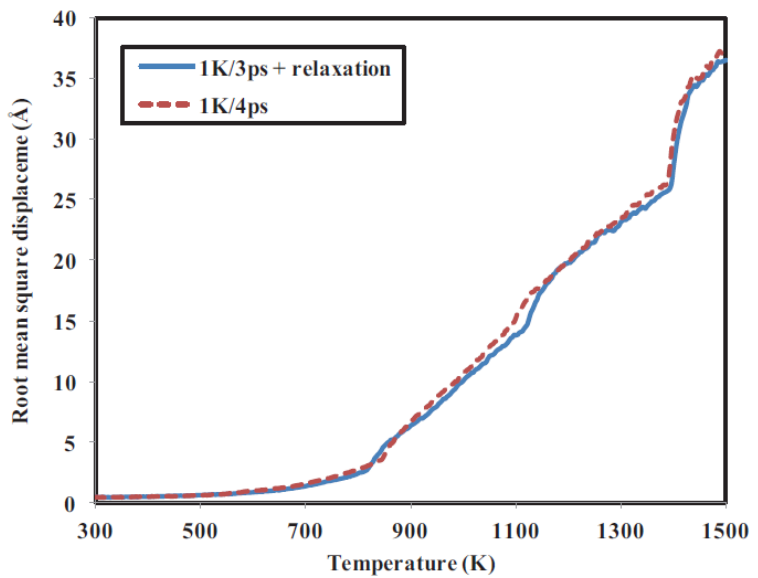
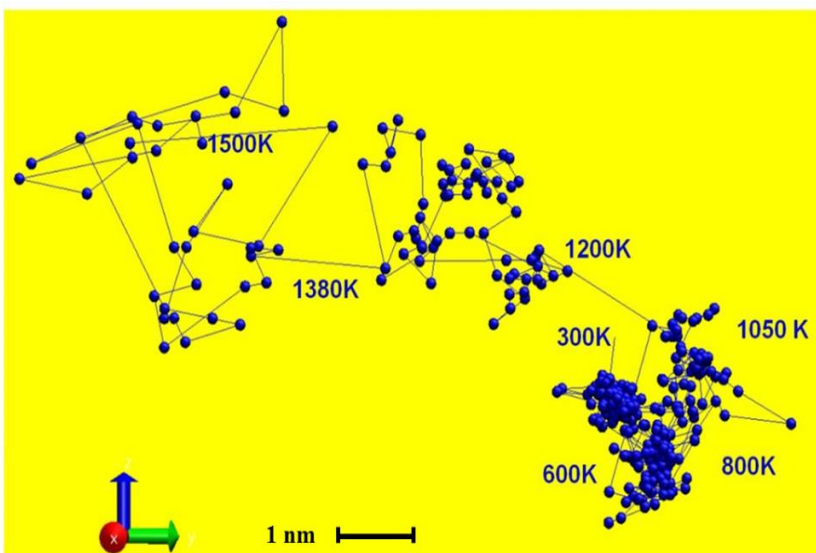


Fig. 4. The comparison of the total root mean square displacement against the temperature between the two annealing methods at the slowest annealing rates.



## Cluster coalescence/melting around 700°C

Above 700°C, staircase structure of RMSD corresponding to stepwise cluster melting

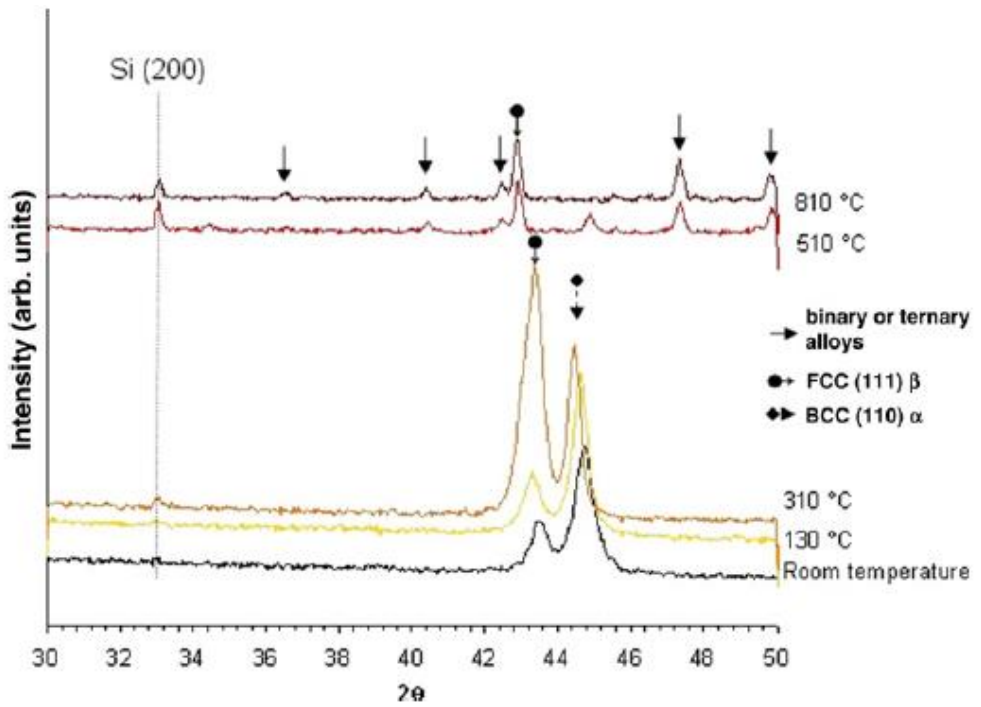
→ consistent with thermal relaxation time: ps range

→ consistent with experiment (Temperature resolved XRD : 600°C)

L. Xie, P. Brault, A.-L. Thomann, J.-M. Bauchire, *AlCoCrCuFeNi high entropy alloy cluster growth and annealing on silicon: A classical molecular dynamics simulation study*, Appl. Surf. Sci. 285P (2013) 810

# HEA : AlCoCrCuFeNi

## Temperature Controlled XRD



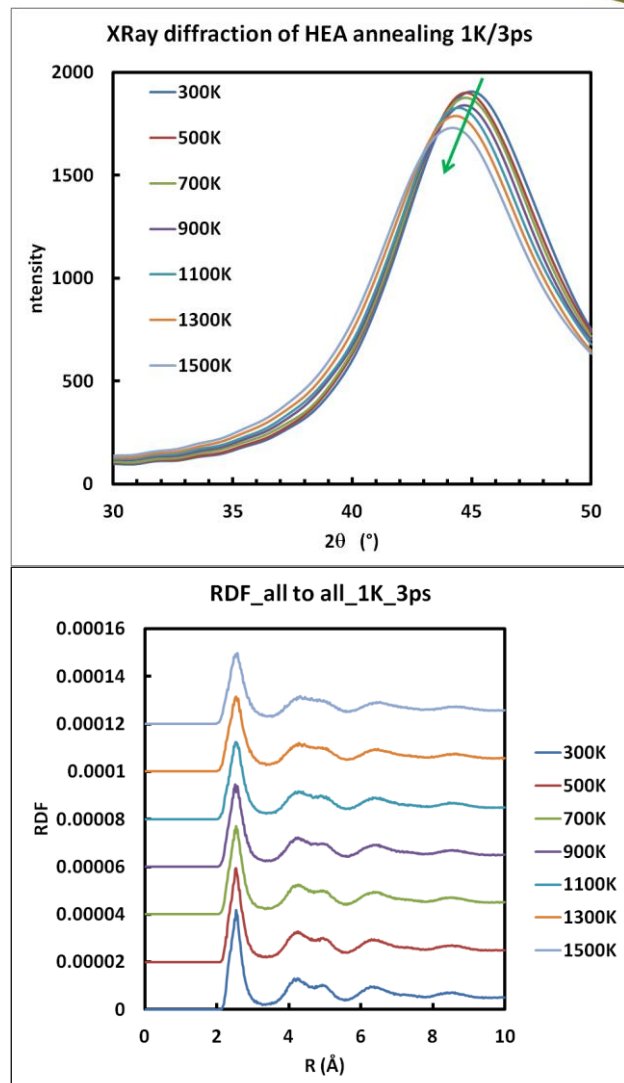
### Temperature XRD

V. Dolique et al, Surface & Coatings Technology 204 (2010) 1989–1992

### Comparison between Experiments and Simulations

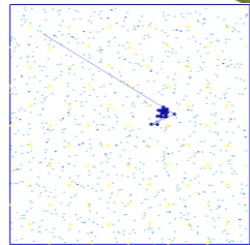
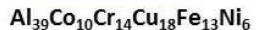
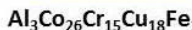
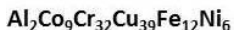
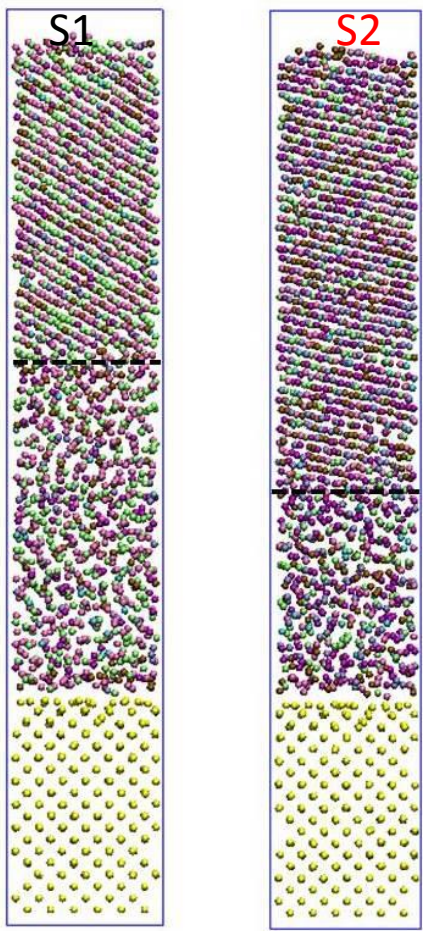
Transition bcc  $\rightarrow$  fcc when  $T^\circ$  increases

No crystallisation

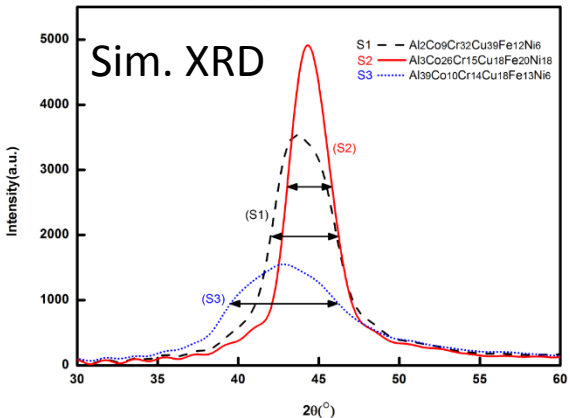
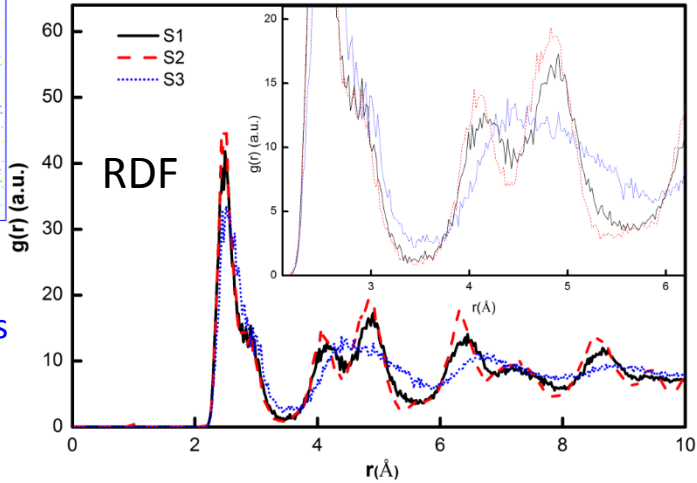


# HEA : AlCoCrCuFeNi Thin film growth

● Al, ● Co, ● Cr, ● Cu, ● Fe, ● Ni, ● Si



Low diffusion  
small substrates  
↓  
thin film



Composition => Important effect on the structure

L. Xie, P. Brault, J.-M. Bauchire, A.-L. Thomann, L. Bedra , *Molecular Dynamics simulations of clusters and thin film growth in the context of plasma sputtering deposition*, J. Phys D 47 (2014) 224004

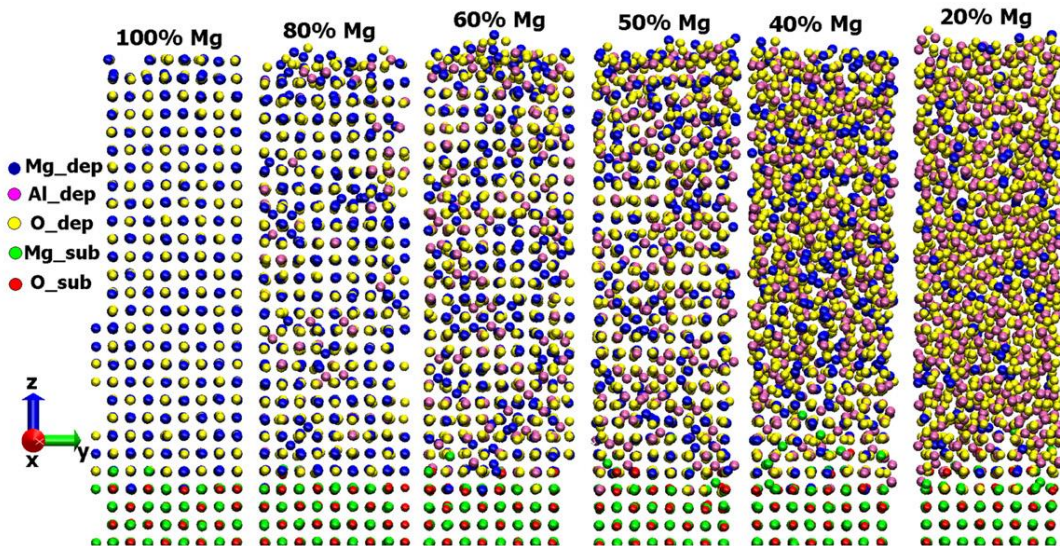
L. Xie, P. Brault, A.-L. Thomann, X. Yang, Y. Zhang, G. Y. Shang, *Molecular Dynamics Simulation of Al-Co-Cr-Cu-Fe-Ni high entropy alloy thin film growth*, Intermetallics 68 (2016) 78

## $Mg_xAl_yO_z$ thin films grown on a MgO (100) and amorphous $Al_2O_3/MgO(100)$

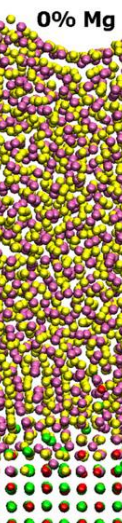
$$V_{ij} = \frac{q_i q_j}{4\pi\epsilon_0 r_{ij}} + A \exp\left(-\frac{r_{ij}}{\rho}\right) - \frac{C}{r_{ij}^6}$$

Two potential sets with full (FC) and partial (PC) charges

Difficulty : long-range interaction → Ewald summation

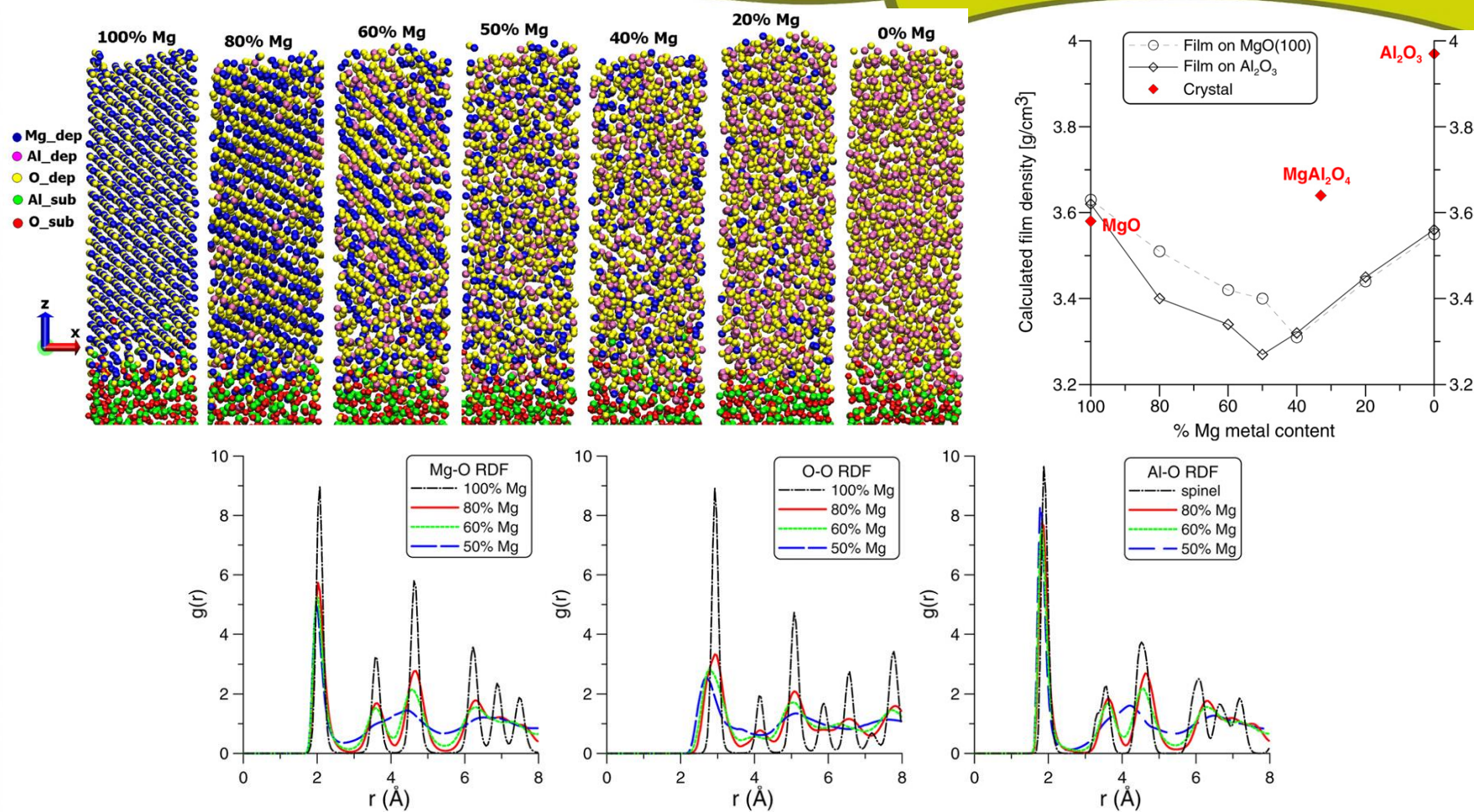


$i-j$		A (eV)	$\rho$ (Å)	C (Å <sup>6</sup> eV)
$Mg^{2+}-O^{2-}$	FC	1279.69	0.29969	0.0
$Al^{3+}-O^{2-}$		1374.79	0.3013	0.0
$O^{2-}-O^{2-}$		9547.96	0.21916	32.0
$Mg^{0.945+}-O^{0.945-}$	PC	32 586	0.178	27.32
$Al^{1.4175+}-O^{0.945-}$		28 480	0.172	34.63
$O^{0.945-}-O^{0.945-}$		6463.4	0.276	85.22
$Mg^{0.945+}-Mg^{0.945+}$		17 650 254	0.080	8.76
$Mg^{0.945+}-Al^{1.4175+}$		22 981 293	0.074	11.10
$Al^{1.4175+}-Al^{1.4175+}$		31 574 470	0.068	14.07



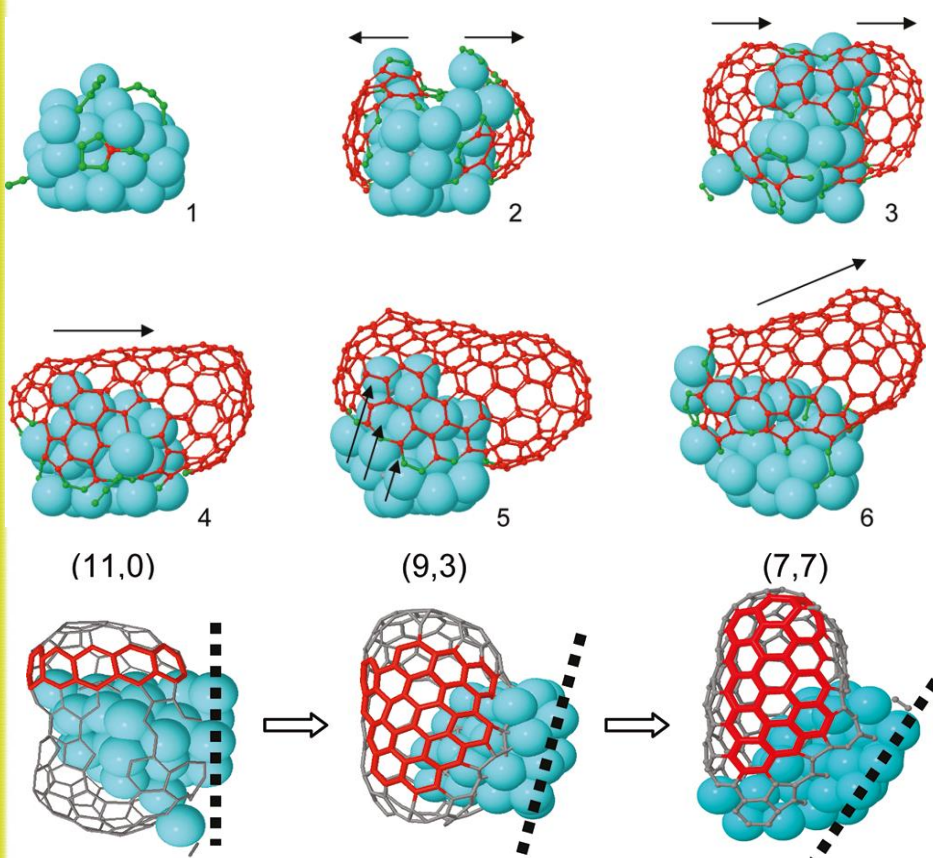
Snapshots of  $Mg_xAl_yO_z$  thin films on MgO(100) using FC potential: compared successfully to sputtering exp.

V Georgieva, M Saraiva, N Jehanathan, O I Lebelev, D Depla and A Bogaerts, Sputter-deposited Mg-Al-O thin films: linking molecular dynamics simulations to experiments, J. Phys. D: Appl. Phys. 42 (2009) 065107



Snapshots, RDF and calculated film density of  $\text{Mg}_x\text{Al}_y\text{O}_z$  thin films on (amorphous  $\text{Al}_2\text{O}_3$ )/ $\text{MgO}(100)$  using FC potential: compared successfully to sputtering exp.

C deposition on Ni NP at 1000 K  
ReaxFF, dt = 0.25 fs

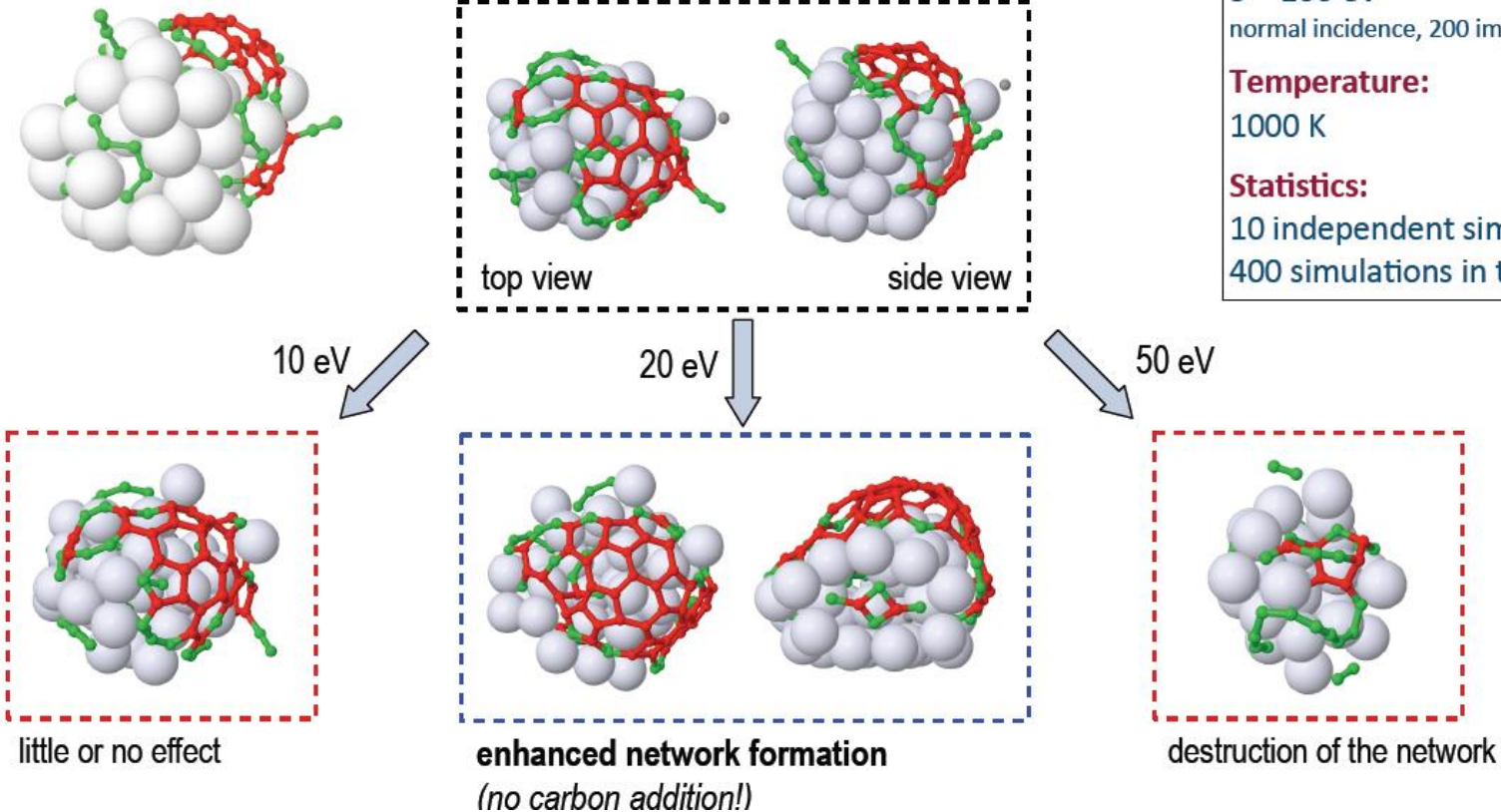


Simulated growth evolution. Arrows indicate the growth or elongation direction of the carbon network. (1) Carbon dissolution and first pentagon formation. (2) Two graphitic patches are formed. (3) These graphitic patches develop into two small caps. First "chirality" is visible (not metallic). (4) The carbon network slides over the cluster. In this process, one cap grows while the other cap disappears. Here, the chirality is changing. This step takes a very long time. (5) The carbon keeps on moving over the metal cluster until part of the metal is freed from the network (indicated by the arrows pointing upward), allowing new C-atoms to be incorporated. (6) At the end of the sliding process, the final chirality is obtained. (i.e., (7,7) metallic)

Evolution of chirality during the growth process. The chirality of the different structures, as defined by its diameter and chiral angle, is indicated above each structure. The dotted line indicates the surface

# PECVD of CNT growth on Ni particles Ion energy effect

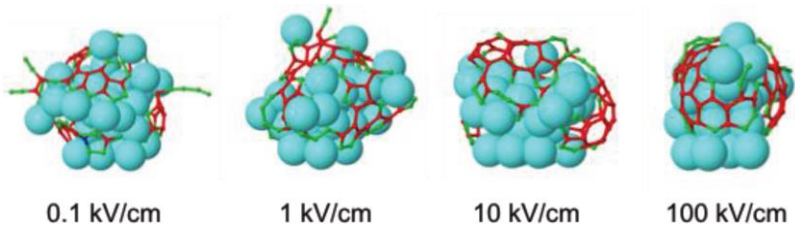
# Nucleation



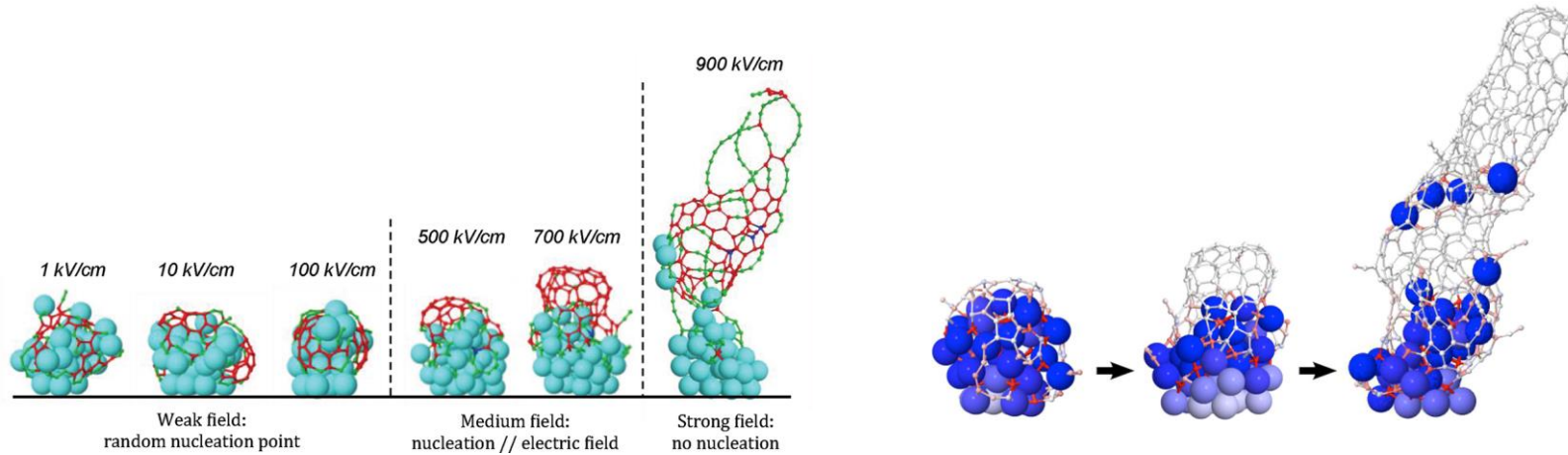
E. C. Neyts, K. Ostrikov, Z. J. Han, S. Kumar, A. C. T. van Duin, and A. Bogaerts, *Defect Healing and Enhanced Nucleation of Carbon Nanotubes by Low-Energy Ion Bombardment*, Phys. Rev. Lett. 110 (2013) 065501

# PECVD of CNT growth on Ni particles

## Electric field effects



Effect of increasing the electric field value in the range 0.1–100 kV/cm on the structure and ordering of the nucleating carbon network. The small red atoms are 3-coordinated carbon atoms, the small green atoms are 2- or 1-coordinated carbon atoms. The large atoms represent nickel atoms.



Effect of applying an electric field on the nucleation of a SWNT cap

E. C. Neyts, A. C. T. van Duin, A. Bogaerts, *Insights in the Plasma-Assisted Growth of Carbon Nanotubes through Atomic Scale Simulations: Effect of Electric Field*, J. Am. Chem. Soc. 134 (2012) 1256

## ❑ Conclusion

MD is appropriate for insight into basic mechanisms of sputtering, plasma phase reactions and deposition, provided close matching to experiments is achieved: Especially initial conditions and energy treatment during interactions.

## ❑ Challenging perspectives

Investigation of the reactive (sputtering) processes at the molecular scale on surfaces or in plasma/gas phase

Complex oxide materials plasma and deposition: beyond pair potentials

Complex substrates (porous, ...)

Coupling MDS of sputtering and deposition to reactor models

Suitable potential (ReaxFF, COMB, REBO, ...)

**Many thanks for your attention**